Vasohibins/SVBP are tubulin carboxypeptidases (TCPs) that regulate neuron differentiation

Chrystelle Aillaud, Christophe Bosc, Leticia Peris, Anouk Bosson, Pierre Heemeryck, Juliette van Dijk, Julien Le Friec, Benoit Boulan, Frédérique Vossier, Laura E. Sanman, et al.

Science AAAS

Accepted Manuscript
published in Science, 16 Nov 2017,Vol 358, Issue 6369, pp. 1448-1453
DOI: 10.1126/science.aao4165

Title:

Vasohibins/SVBP are tubulin carboxypeptidases (TCP) that regulate neuron differentiation

Authors:

Chrystelle Aillaud[1,2], Christophe Bosc[1,2], Leticia Peris[1,2], Anouk Bosson[1,2], Pierre Heemeryck[1,2], Juliette Van Dijk[3,4], Julien Le Friec[1,2], Benoit Boulan[1,2], Frédérique Vossier[1,2], Laura E. Sanman[5], Salahuddin Syed[5], Neri Amara[5], Yohann Couté[6], Laurence Lafanechère[7], Eric Denarier[1,2,8], Christian Delphin[1,2], Laurent Pelletier[1,2], Sandrine Humbert[1,2], Matthew Bogyo[5], Annie Andrieux*[1,2,8†], Krzysztof Rogowski*[3†], and Marie-Jo Moutin*[1,2].

Affiliations :

[1]Univ. Grenoble Alpes, Grenoble Institut des Neurosciences, GIN, F-38000 Grenoble, France

[2]Inserm, U1216, F-38000 Grenoble, France.

[3]CNRS UMR9002, Institut de Génétique Humaine, IGH, Univ. Montpellier, 34000 Montpellier, France.

[4]CNRS UMR5237, Centre de Recherche en Biochimie Macromoléculaire, CRBM, Univ. Montpellier, 34000 Montpellier, France.

[5]Department of Pathology, Stanford University School of Medicine, Stanford, California 94305, USA.

[6]Univ. Grenoble Alpes, CEA, INSERM, BIG-BGE, F-38000 Grenoble, France.

[7]Team Regulation & Pharmacology of the Cytoskeleton, Institute for Advanced Biosciences, INSERM U 1209, CNRS UMR 5309, Univ. Grenoble Alpes, 38000 Grenoble, France.

[8]CEA, BIG-GPC, F-38000 Grenoble, France.

*Correspondence to: moutinm@univ-grenoble-alpes.fr, annie.andrieux@univ-grenoble-alpes.fr, or krzysztof.rogowski@igh.cnrs.fr.

†These authors contributed equally to this work

Abstract:

Reversible detyrosination of α-tubulin is crucial to microtubule dynamics and functions and defects have been implicated in cancer, brain disorganization and cardiomyopathies. The identity of the tubulin tyrosine carboxypeptidase (TCP) responsible for detyrosination has remained unclear. We used chemical proteomics with a potent unique irreversible inhibitor to show that the major brain TCP is a complex of vasohibin-1 (VASH1) with the Small Vasohibin Binding Protein (SVBP). VASH1 and its homologue VASH2, when complexed with SVBP, exhibited robust and specific Tyr/Phe carboxypeptidase activity on microtubules. Knock down of vasohibins or SVBP and/or inhibitor addition in cultured neurons reduced detyrosinated α-tubulin levels and caused severe differentiation defects. Furthermore, knock down of vasohibins disrupted neuronal migration in developing mouse neocortex. Thus vasohibin/SVBP complexes represent long sought TCP enzymes.

One sentence summary:

Vasohibins complexed to SVBP detyrosinate α-tubulin and play a role in neuron polarization and brain cortex development.

Main text:

Microtubules are cytoskeletal polymers of α/β tubulin dimers centrally involved in cell division, motility and morphogenesis. In the detyrosination/tyrosination cycle of tubulin, the C-terminal tyrosine of α-tubulin is removed by an elusive peptidase (TCP) and re-added by the tubulin tyrosine ligase (TTL, for review see (*1*)). This cycle, which is unique to tubulin and mostly conserved from chordates to mammals, has a vital role in vivo (*2*). Tubulin de/tyrosination of α-tubulin is an important regulatory signal for mitosis (*3-5*), for neuronal physiology (*6-8*), and for muscle mechanotransduction (*9, 10*). Consequently, abnormal tyrosination levels are associated with cell transformation and tumor aggressiveness (*11, 12*), neuronal disorganization (*2*), and heart failure and cardiomyopathies (*10, 13*). Although the detyrosination reaction was first described 40 years ago (*14*), the identity of TCP has remained unknown.

To enrich for TCP, we designed a three step purification procedure using taxol-stabilized radiolabelled tyrosinated microtubules as a substrate to follow activity. A typical procedure gave a final purification factor of nearly 400-fold (Figs. 1A and S1A). The last fraction (IV) was able to cleave the C-terminal tyrosine from tubulin incorporated in microtubules but not from EB1 (Fig. S1B). EB1 is a protein that shares a similar C-terminal sequence with α-tubulin (-QEEY instead of -GEEY) and is generally not a substrate for TCP in physiological contexts (*15*).

To isolate the protein(s) responsible for TCP activity from fraction IV, we reasoned that an irreversible inhibitor could be used as in other chemical proteomic studies (*16*). We tested the sensitivity of brain TCP to various commercial protease inhibitors. The activity was inhibited by several serine/cysteine protease inhibitors (AEBSF, TLCK, TPCK, E-64, parthenolide) and by the thiol-reactive compound N-Ethylmaleimide (Figs. S2A and 1B). These results, in agreement with prior studies (*17*), strongly suggested that the catalytic activity of the putative TCP depends on a catalytic cysteine.

Although E-64 only showed modest inhibitory activity (IC_{50} around 300 µM, Fig. 1B), it is an ideal starting point for inhibitor design because its reactive epoxide electrophile can display a peptide or amino acid mimicking native protein C-terminus. Furthermore, parthenolide, which is widely used to down-regulate detyrosination levels in cells (*4, 6, 9, 10*), contains an epoxide function which is essential to its cellular effect (*17*). We thus synthesized three inhibitors, epoY, epoEY and epoEEY, which contain the epoxide coupled to one, two or three amino-acids from the α-tubulin C-terminus (Fig. S2B). EpoY was the most potent inhibitor of the TCP activity (IC_{50} around 500 nM, Fig. 1B). Alkyne-epoY, which retained a strong inhibitory potency (Fig. 1B, C) and irreversibly inhibited the activity (Fig. S2C, D), was used to perform TAMRA labeling of fraction IV by click chemistry (Fig. 1D). This labeling showed specific modification of a small number of proteins (Fig. 1E). We then purified the inhibitor targets using agarose beads and, after on-beads trypsin digestion and quantitative mass spectrometry analyses of the resulting peptides from three independent experiments, we identified the protein vasohibin-1 (VASH1) as the most likely TCP candidate (Fig 1D, Tables S1-S2). Peptides covering the almost full VASH1 sequence were detected (Fig. S2E). Furthermore, recent bioinformatics data show that Vasohibin-1 and its homologue vasohibin-2 (VASH2) possess a non-canonical Cys-His-Ser catalytic triad and are members of the transglutaminase-like cysteine proteases family (*18*) (Fig. 1F).

Vasohibin proteins (41-42 kDa) have been extensively characterized as angiogenesis regulators but are poorly understood on a molecular level (*19*). SVBP (Ccdc23) is a high affinity binding partner of vasohibins that has a chaperone-like function (*20*). We examined the ability of VASH proteins to detyrosinate α-tubulin in cells in the absence or presence of SVBP. Expression of vasohibins alone in HEK293T cells resulted in a slight increase of detyrosinated tubulin, whereas expression of either protein with SVBP resulted in a substantial increase in detyrosinated tubulin corresponding to a nearly complete loss of endogenous tyrosinated tubulin (Fig. 2A). Mutation of the putative catalytic cysteine on vasohibins (C179A for VASH1, and C158A for VASH2 (*18*))

abolished their capacity to produce detyrosinated tubulin. Similarly, in murine embryonic fibroblasts (MEF), expression of the vasohibins with SVBP resulted in complete detyrosination of endogenous α-tubulin (Figs. 2B and S3A).

Alpha-tubulins are generally encoded with a C-terminal tyrosine preceded by two glutamates. Alpha4-tubulin lacks the C-terminal tyrosine and α8-tubulin contains a C-terminal phenylalanine residue. Phenylalanine can be incorporated in place of tyrosine in tubulin and be a possible cause of neuronal dysfunction (*21*). We tested the substrate specificity of the vasohibins by overexpressing α1B- and α8-tubulin together with VASH1 or VASH2 and SVBP in HEK293T cells. Both tubulin isotypes were cleaved by active vasohibins when expressed with SVBP (Figs. 2C and S3B). Vasohibins were unable to cleave the C-terminal residue when tyrosine was mutated to alanine (Figs. 2C and S3B), confirming the specificity of VASH proteins for C-terminal tyrosine and phenylalanine residues.

We overexpressed vasohibins in HEK293T cells in the absence or presence of SVBP and purified the resulting complexes using a cobalt resin. SVBP co-purified with both vasohibins as expected from previous affinity measurements, (K_D 30-90 nM (*20*)), and complex formation was not dependent on catalytic activity (Fig. S4A). The two protein complexes efficiently catalyzed tubulin detyrosination while complexes containing the catalytic dead versions of the vasohibins were unable to detyrosinate tubulin (Fig. 2D). Both complexes cleaved microtubules more rapidly compared to tubulin dimers (Fig. 2E, S4B), consistent with the reported preference of brain TCP in in vitro experiments (*1, 22, 23*). Purified VASH1/SVBP complex was not able to cleave the C-terminal tyrosine from EB1 indicating its clear tubulin preference. Intringuingly VASH2/SVBP complex was able to partially detyrosinate EB1 in the same conditions (Fig. 2F). In most cell types, including neuronal-derived, C-terminal tyrosine cleavage is restricted to tubulin (*1, 15*). EB1 can however be detyrosinated in specific endothelial and tumor cells (*24*) and this may be related to their VASH2 contents or defect in a regulatory mechanism.

To confirm the functional significance of vasohibins and their role in α-tubulin detyrosination, we assessed the phenotypic effects of knocking down expression of these proteins in differentiating neurons where the de/tyrosination cycle is highly important for growth cone pathfinding and axon differentiation, i. e. for neuron polarization (*2, 7, 8*). Although we were unable to detect vasohibins and SVBP by immuno-blot in mouse neurons using commercial antibodies, we amplified their transcripts from RNA preparations of cultured hippocampal neurons as well as of adult and embryonic mouse brain tissues (Fig. 3A, S5A, S6A). We transfected hippocampal neurons with plasmids expressing short hairpin RNAs (shRNAs) targeting either the vasohibins or SVBP (validated in Fig. S5B and S6B) as well as control shRNAs. The levels of detyrosinated α-tubulin were decreased by almost 50 % when the two vasohibins, or the SVPB, were down-regulated. Addition of inhibitor (alkyne-epoY) also largely reduced detyrosinated α-tubulin (Fig. 3B, C, S5C). When added together with the shRNAs, levels of detyrosinated tubulin were decreased up to 75 % (Fig. 3B, C). The remaining pool of detyrosinated α-tubulin could be due to uncomplete depletion of vasohibins activities or to the presence of α4-tubulin which genetically lacks the C-terminal tyrosine and remains in detyrosinated form in the brain (*25*). The occurrence of other detyrosinases can however not be excluded. Confocal images of neurons cultured 2 days in vitro (2DIV) confirmed a decrease in the levels of the native detyrosinated α-tubulin upon reduction or inhibition of vasohibins expression (Fig. 3D). The remaining detyrosinated pools were specifically concentrated in the axon, while α-tubulin in the other neurites appeared highly tyrosinated. Vasohibins down-regulation led to a clear delay in axonal differentiation (Fig. 3E). Tau and ankyrin G staining of neurons bearing an axon confirmed normal distribution, with Tau highly expressed in axon shaft at 3DIV and ankyrin G in the axon initial segment at 10DIV (Fig. S7). 2DIV neurons knocked down for vasohibins developed an increased number of neurites and branches with overall reduced axon length (Fig. 3F). A delay of axon differentiation and similar morphological anomalies were observed when down-regulating SVBP (Fig. S6D-F). Transfection of a plasmid allowing

coexpression of shRNAs targeting SVBP and a shRNA-resistant form of SVBP rescued α-tubulin detyrosination levels (Fig. S6A, C). Thus, contrary to the premature axonal differentiation observed in the absence of the reverse enzyme TTL (*2*), here we observe a clear delay of axon differentiation when down-regulating vasohibins or SVBP.

We next tested the functional significance of vasohibins in vivo in mouse brain and focused on the cerebral cortex where the de/tyrosination cycle is critical for the neocortex layer organization (*2*). During corticogenesis neuronal migration relies in part on neuron polarization which was highly dependent on vasohibins (Fig. 3D, E) and SVBP (Fig. S6D, E). We electroporated E14.5 embryos with the plasmids expressing shRNAs targeting the vasohibins as well as control shRNA, and analyzed radial neuronal migration four days later. At E18.5, most neurons from control brains had reached the upper layer (bin 1), whereas when vasohibins were downregulated a significant fraction of neurons failed to do so (Fig 4A, B). Thus, these enzymes have a crucial role in neuronal migration during brain cortex development.

TCP remained the crucial missing element of the α-tubulin de/tyrosination cycle for 40 years. Here, we identify vasohibins as enzymatic proteins that perform the TCP function (Fig. S8). The failure of prior attempts to identify TCPs most probably resulted from their association with SVBP for stability and activity which could likely be lost during standard purification assays. In agreement with TCP functions, vasohibins are widely distributed in eucaryotes, have broad tissue expression, and vasohibin-1 (which is generally more expressed than vasohibin-2) is abundant in brain, heart and kidney (*18, 26, 27*) (see also GTEx Portal on https://www.gtexportal.org/home/). Additionally, we demonstrated their critical role in neuron and brain physiology.

References and notes:

1. H. S. Barra, C. A. Arce, C. E. Argarana, Posttranslational tyrosination/detyrosination of tubulin. *Molecular neurobiology* **2**, 133-153 (1988).

2. C. Erck, L. Peris, A. Andrieux, C. Meissirel, A. D. Gruber, M. Vernet, A. Schweitzer, Y. Saoudi, H. Pointu, C. Bosc, P. A. Salin, D. Job, J. Wehland, A vital role of tubulin-tyrosine-ligase for neuronal organization. *Proceedings of the National Academy of Sciences of the United States of America* **102**, 7853-7858 (2005).

3. A. C. Badin-Larcon, C. Boscheron, J. M. Soleilhac, M. Piel, C. Mann, E. Denarier, A. Fourest-Lieuvin, L. Lafanechere, M. Bornens, D. Job, Suppression of nuclear oscillations in Saccharomyces cerevisiae expressing Glu tubulin. *Proceedings of the National Academy of Sciences of the United States of America* **101**, 5577-5582 (2004).

4. M. Barisic, R. Silva e Sousa, S. K. Tripathy, M. M. Magiera, A. V. Zaytsev, A. L. Pereira, C. Janke, E. L. Grishchuk, H. Maiato, Mitosis. Microtubule detyrosination guides chromosomes during mitosis. *Science (New York, N.Y* **348**, 799-803 (2015).

5. L. Peris, M. Thery, J. Faure, Y. Saoudi, L. Lafanechere, J. K. Chilton, P. Gordon-Weeks, N. Galjart, M. Bornens, L. Wordeman, J. Wehland, A. Andrieux, D. Job, Tubulin tyrosination is a major factor affecting the recruitment of CAP-Gly proteins at microtubule plus ends. *The Journal of cell biology* **174**, 839-849 (2006).

6. P. Gobrecht, A. Andreadaki, H. Diekmann, A. Heskamp, M. Leibinger, D. Fischer, Promotion of Functional Nerve Regeneration by Inhibition of Microtubule Detyrosination. *J Neurosci* **36**, 3890-3902 (2016).

7. Y. Konishi, M. Setou, Tubulin tyrosination navigates the kinesin-1 motor domain to axons. *Nat Neurosci* **12**, 559-567 (2009).

8. S. Marcos, J. Moreau, S. Backer, D. Job, A. Andrieux, E. Bloch-Gallego, Tubulin tyrosination is required for the proper organization and pathfinding of the growth cone. *PloS one* **4**, e5405 (2009).

9. J. P. Kerr, P. Robison, G. Shi, A. I. Bogush, A. M. Kempema, J. K. Hexum, N. Becerra, D. A. Harki, S. S. Martin, R. Raiteri, B. L. Prosser, C. W. Ward, Detyrosinated

microtubules modulate mechanotransduction in heart and skeletal muscle. *Nature communications* **6**, 8526 (2015).

10. P. Robison, M. A. Caporizzo, H. Ahmadzadeh, A. I. Bogush, C. Y. Chen, K. B. Margulies, V. B. Shenoy, B. L. Prosser, Detyrosinated microtubules buckle and bear load in contracting cardiomyocytes. *Science (New York, N.Y* **352**, aaf0659 (2016).
11. L. Lafanechere, C. Courtay-Cahen, T. Kawakami, M. Jacrot, M. Rudiger, J. Wehland, D. Job, R. L. Margolis, Suppression of tubulin tyrosine ligase during tumor growth. *Journal of cell science* **111 (Pt 2)**, 171-181 (1998).
12. R. A. Whipple, M. A. Matrone, E. H. Cho, E. M. Balzer, M. I. Vitolo, J. R. Yoon, O. B. Ioffe, K. C. Tuttle, J. Yang, S. S. Martin, Epithelial-to-mesenchymal transition promotes tubulin detyrosination and microtentacles that enhance endothelial engagement. *Cancer Res* **70**, 8127-8137 (2010).
13. S. Belmadani, C. Pous, R. Ventura-Clapier, R. Fischmeister, P. F. Mery, Post-translational modifications of cardiac tubulin during chronic heart failure in the rat. *Molecular and cellular biochemistry* **237**, 39-46 (2002).
14. M. E. Hallak, J. A. Rodriguez, H. S. Barra, R. Caputto, Release of tyrosine from tyrosinated tubulin. Some common factors that affect this process and the assembly of tubulin. *FEBS Lett* **73**, 147-150 (1977).
15. A. Bosson, J. M. Soleilhac, O. Valiron, D. Job, A. Andrieux, M. J. Moutin, Cap-Gly proteins at microtubule plus ends: is EB1 detyrosination involved? *PloS one* **7**, e33490 (2012).
16. M. A. Child, C. I. Hall, J. R. Beck, L. O. Ofori, V. E. Albrow, M. Garland, P. W. Bowyer, P. J. Bradley, J. C. Powers, J. C. Boothroyd, E. Weerapana, M. Bogyo, Small-molecule inhibition of a depalmitoylase enhances Toxoplasma host-cell invasion. *Nat Chem Biol* **9**, 651-656 (2013).

17. X. Fonrose, F. Ausseil, E. Soleilhac, V. Masson, B. David, I. Pouny, J. C. Cintrat, B. Rousseau, C. Barette, G. Massiot, L. Lafanechere, Parthenolide inhibits tubulin carboxypeptidase activity. *Cancer Res* **67**, 3371-3378 (2007).

18. L. Sanchez-Pulido, C. P. Ponting, Vasohibins: new transglutaminase-like cysteine proteases possessing a non-canonical Cys-His-Ser catalytic triad. *Bioinformatics* **32**, 1441-1445 (2016).

19. Y. Sato, The vasohibin family: a novel family for angiogenesis regulation. *Journal of biochemistry* **153**, 5-11 (2013).

20. Y. Suzuki, M. Kobayashi, H. Miyashita, H. Ohta, H. Sonoda, Y. Sato, Isolation of a small vasohibin-binding protein (SVBP) and its role in vasohibin secretion. *Journal of cell science* **123**, 3094-3101 (2010).

21. Y. Ditamo, Y. M. Dentesano, S. A. Purro, C. A. Arce, C. G. Bisig, Post-Translational Incorporation of L-Phenylalanine into the C-Terminus of alpha-Tubulin as a Possible Cause of Neuronal Dysfunction. *Scientific reports* **6**, 38140 (2016).

22. G. G. Deanin, S. F. Preston, R. K. Hanson, M. W. Gordon, On the mechanism of turnover of the carboxy-terminal tyrosine of the alpha chain of tubulin. *Eur J Biochem* **109**, 207-216 (1980).

23. N. Kumar, M. Flavin, Preferential action of a brain detyrosinolating carboxypeptidase on polymerized tubulin. *The Journal of biological chemistry* **256**, 7678-7686 (1981).

24. A. Rovini, G. Gauthier, R. Berges, A. Kruczynski, D. Braguer, S. Honore, Anti-migratory effect of vinflunine in endothelial and glioblastoma cells is associated with changes in EB1 C-terminal detyrosinated/tyrosinated status. *PloS one* **8**, e65694 (2013).

25. V. Redeker, Mass spectrometry analysis of C-terminal posttranslational modifications of tubulins. *Methods Cell Biol* **95**, 77-103 (2010).

26. S. Nimmagadda, P. Geetha-Loganathan, F. Prols, M. Scaal, B. Christ, R. Huang, Expression pattern of Vasohibin during chick development. *Dev Dyn* **236**, 1358-1362 (2007).

27. T. Shibuya, K. Watanabe, H. Yamashita, K. Shimizu, H. Miyashita, M. Abe, T. Moriya, H. Ohta, H. Sonoda, T. Shimosegawa, K. Tabayashi, Y. Sato, Isolation and characterization of vasohibin-2 as a homologue of VEGF-inducible endothelium-derived angiogenesis inhibitor vasohibin. *Arteriosclerosis, thrombosis, and vascular biology* **26**, 1051-1057 (2006).

28. S. Ramirez-Rios, E. Denarier, E. Prezel, A. Vinit, V. Stoppin-Mellet, F. Devred, P. Barbier, V. Peyrot, C. L. Sayas, J. Avila, L. Peris, A. Andrieux, L. Serre, A. Fourest-Lieuvin, I. Arnal, Tau antagonizes end-binding protein tracking at microtubule ends through a phosphorylation-dependent mechanism. *Molecular biology of the cell* **27**, 2924-2934 (2016).

29. C. E. Argarana, H. S. Barra, R. Caputto, Tubulinyl-tyrosine carboxypeptidase from chicken brain: properties and partial purification. *Journal of neurochemistry* **34**, 114-118 (1980).

30. J. Milbradt, A. Kraut, C. Hutterer, E. Sonntag, C. Schmeiser, M. Ferro, S. Wagner, T. Lenac, C. Claus, S. Pinkert, S. T. Hamilton, W. D. Rawlinson, H. Sticht, Y. Coute, M. Marschall, Proteomic analysis of the multimeric nuclear egress complex of human cytomegalovirus. *Mol Cell Proteomics* **13**, 2132-2146 (2014).

31. J. D. Pedelacq, S. Cabantous, T. Tran, T. C. Terwilliger, G. S. Waldo, Engineering and characterization of a superfolder green fluorescent protein. *Nat Biotechnol* **24**, 79-88 (2006).

32. I. Arganda-Carreras, R. Fernandez-Gonzalez, A. Munoz-Barrutia, C. Ortiz-De-Solorzano, 3D reconstruction of histological sections: Application to mammary gland tissue. *Microsc Res Tech* **73**, 1019-1029 (2010).

33. M. Barnat, J. Le Friec, C. Benstaali, S. Humbert, Huntingtin-Mediated Multipolar-Bipolar Transition of Newborn Cortical Neurons Is Critical for Their Postnatal Neuronal Morphology. *Neuron* **93**, 99-114 (2017).

34. V. K. Khodiyar, L. J. Maltais, B. J. Ruef, K. M. Sneddon, J. R. Smith, M. Shimoyama, F. Cabral, C. Dumontet, S. K. Dutcher, R. J. Harvey, L. Lafanechere, J. M. Murray, E. Nogales, D. Piquemal, F. Stanchi, S. Povey, R. C. Lovering, A revised nomenclature for the human and rodent alpha-tubulin gene family. *Genomics* **90**, 285-289 (2007).

35. C. Aillaud, C. Bosc, Y. Saoudi, E. Denarier, L. Peris, L. Sago, N. Taulet, A. Cieren, O. Tort, M. M. Magiera, C. Janke, V. Redeker, A. Andrieux, M. J. Moutin, Evidence for new C-terminally truncated variants of alpha- and beta-tubulins. *Molecular biology of the cell* **27**, 640-653 (2016).

36. L. Paturle-Lafanechere, M. Manier, N. Trigault, F. Pirollet, H. Mazarguil, D. Job, Accumulation of delta 2-tubulin, a major tubulin variant that cannot be tyrosinated, in neuronal tissues and in stable microtubule assemblies. *Journal of cell science* **107 (Pt 6)**, 1529-1543 (1994).

37. K. Rogowski, J. van Dijk, M. M. Magiera, C. Bosc, J. C. Deloulme, A. Bosson, L. Peris, N. D. Gold, B. Lacroix, M. B. Grau, N. Bec, C. Larroque, S. Desagher, M. Holzer, A. Andrieux, M. J. Moutin, C. Janke, A family of protein-deglutamylating enzymes associated with neurodegeneration. *Cell* **143**, 564-578 (2010).

Acknowledgements:

We would like to dedicate this manuscript to Dr Hector Barra, father of the de/tyrosination cycle who passed away on 2nd december 2016. We are grateful to D. Job who strongly supported initiation of the project and for his constant encouragements. We thank M. Comte, E. Martin, C. Corrao, and C. Paoli for technical assistance. We thank members of the PIC-GIN platform for their help in cell imaging and zootechnicians of the Grenoble Institut des Neurosciences for animal care. We thank M. Steinmetz for providing purified TTL, A. Beghin for initial development of AutoNeuriteJ macro. We thank the support of the discovery platform and informatics group at EDyP.

This work was supported by INSERM, CEA, University Grenoble Alpes, CNRS, and by La Ligue Contre le Cancer comités de l'Isère et de Savoie (to MJM), Association pour la Recherche sur le Cancer (SFI20111204053 to MJM; DOC20120605000 to AB; 20151203348 to LL), Fondation pour la Recherche Médicale FDT20160435356 (to CA), ANR-13-JSV2-0002/TYRTUB (to KR), INCA 2016-165 (to LL) and the National Institutes of Health grant R01 EB005011 (to MB). Proteomic experiments were partly supported by the ProFi grant (ANR-10-INBS-08-01).

A patent untitled "Methods and pharmaceutical compositions for treating tubulin carboxypeptidases associated diseases" has been filed by Inserm and UGA.

Data described can be found in the main figures, supplementary materials and auxiliary table.

Supplementary materials:

Materials and Methods

Author contributions

Figs S1 to S7

Table S1

References (28-37)

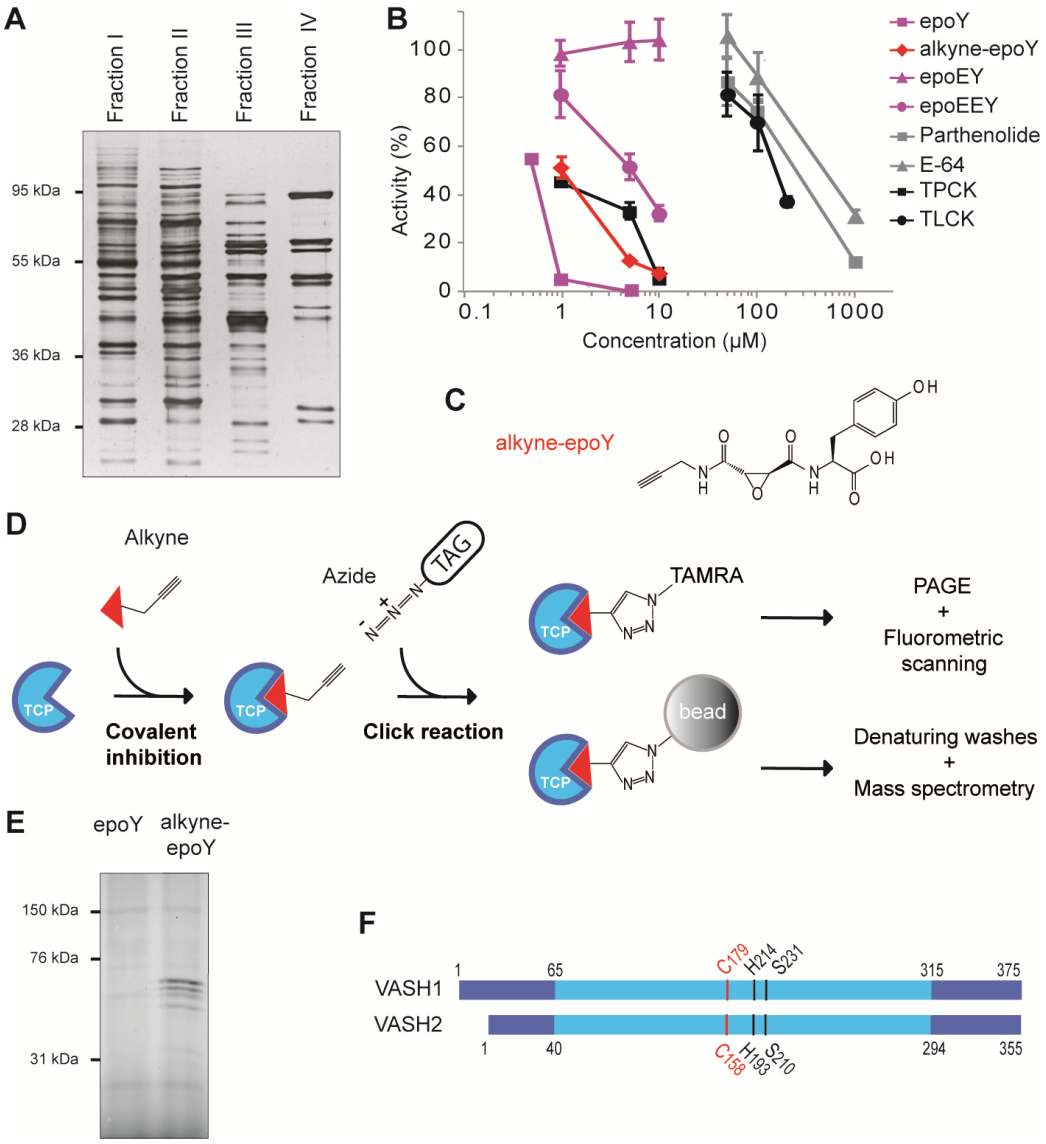

Fig. 1. Purification and identification of mouse brain TCP. (A) SDS-PAGE (silver staining) of the indicated fractions of TCP enrichment from mouse brain (1 µg of proteins): ammonium sulfate precipitation step followed by two ion exchange columns stages (Fig. S1A). **(B)** Fraction IV sensitivity to inhibitors. TPCK (Tosyl phenylalanyl chloromethyl ketone), TLCK (Tosyl-L-lysyl Chloromethyl ketone): commercial serine/cysteine inhibitors containing either a Phe or a Lys residue. Fraction IV activity showed a 100-fold higher sensitivity to TPCK than to TLCK. E-64 is a natural product inhibitor of clan CA cysteine protease. EpoY, epoEY and epoEEY are designed inhibitors containing an epoxide group coupled with Y, EY or EEY amino-acids respectively. Alkyne-epoY is a clickable version of epoY. Results are expressed as percentage of enzyme activity

(radioactivity assay) in the control with DMSO (mean ± SD, n = 3-6). **(C)** Structure of alkyne-epoY. **(D)** Schematic representation of the last steps of TCP identification using Cu-catalyze azide-alkyne cycloaddition (click reaction). **(E)** Labeling of putative TCP from fraction IV by TAMRA red-fluorescent dye using alkyne-epoY (non-clickable epoY is used as control). **(F)** Schematic representation of mouse vasohibin-1 and vasohibin-2 (69% overall sequence homology; 77% for core domains (clear blue boxes)). These putative transglutaminase-like cysteine peptidases contain an unconventional triad of catalytic residues (Cys, His, Ser).

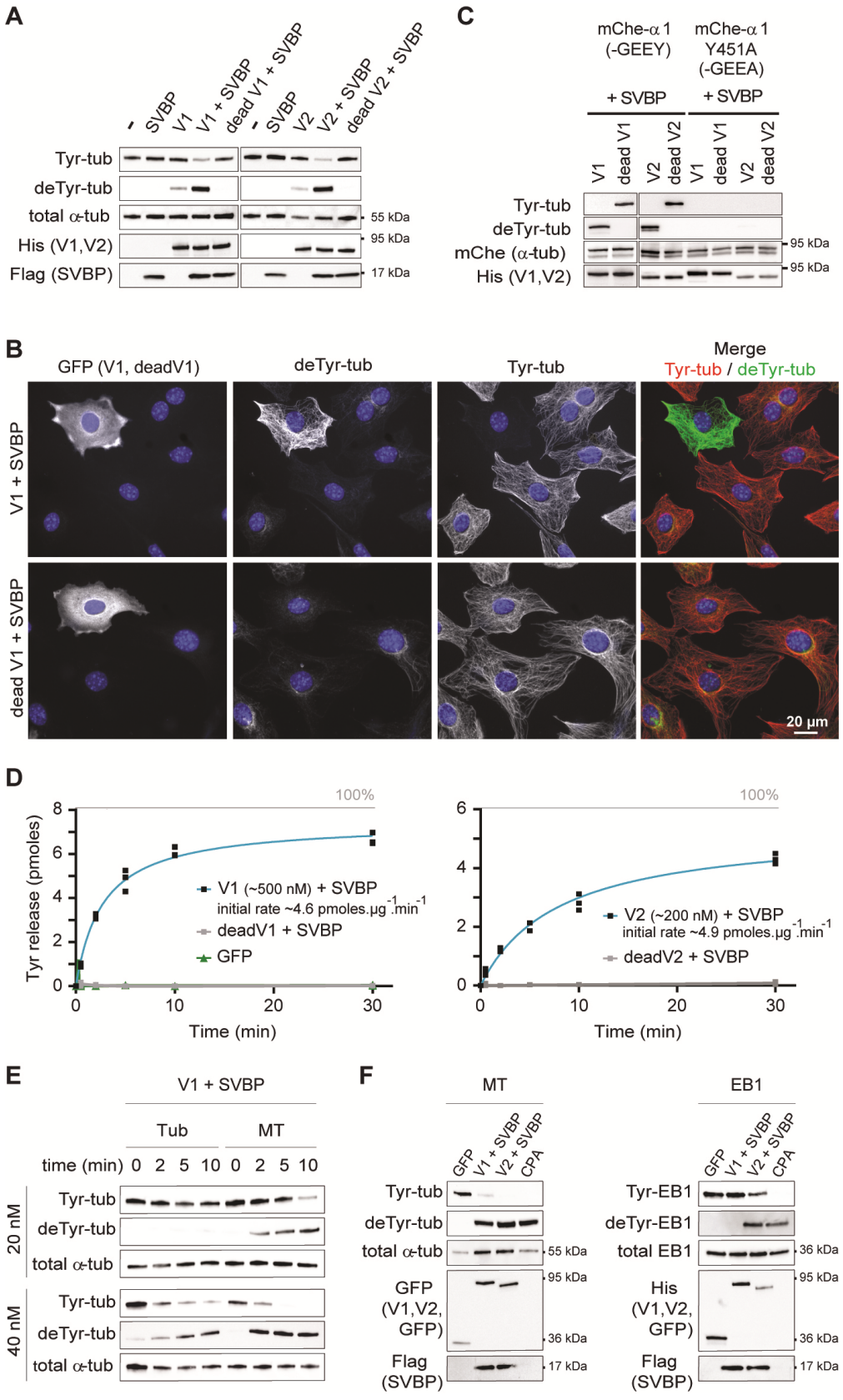

Fig. 2. Vasohibins associated to SVBP are potent tubulin tyrosine carboxypeptidases. (**A**) Immunoblot of endogenous tubulin from HEK293T cells expressing each VASH (V1, V2) or their

dead versions in the absence or presence of exogenous SVBP co-expression. Antibodies specific to tyrosinated and detyrosinated tubulin were used to assess detyrosination. Antibodies to α-tubulin, His and Flag respectively reveal amounts of tubulin, vasohibin and SVBP. Non-transfected cells (-) show endogenous levels of tubulin modifications. **(B)** Immunofluorescence images of de/tyrosinated α-tubulin pools from MEF cells expressing active or inactive VASH1, and SVBP. Vasohibins were probed with anti-GFP antibody. **(C)** Immunoblot of protein extracts from HEK293T cells expressing mCherry-α1B-tubulin, each VASH and SVBP. Native or mutated versions of α1B-tubulin, respectively ending with EEY or EEA, were used. Levels of de/tyrosinated tubulin were measured as in (A). Antibody to mCherry demonstrates same amounts of exogenous α-tubulin. **(D)** Detyrosination activity of purified VASH/SVBP complexes assessed using [^{14}C]-tyrosinated taxol-stabilized microtubules (6-8 μM), n = 3. Active and catalytic dead versions of the vasohibins were coexpressed with SVBP in HEK293T cells and purified on cobalt resin (Fig. S4A). A purified GFP-His construct was used as a control. Data points were fitted with a single exponential (blue line). The theoretical maximal tyrosine release is indicated by a 100% line. **(E)** Detyrosination activity of purified VASH1/SVBP complexes (20 or 40 nM) on brain microtubules or tubulin dimers (5 μM) assessed by immunoblot. We controlled that tubulin was in dimeric or in assembled form (Fig S4C) and that the same amounts of enzymatic complexes were present (Fig S4D). **(F)** Detyrosination activity of purified VASH/SVBP complexes (600 nM) on brain microtubules or recombinant GFP-EB1 (5 μM). Note that enzyme quantities are much higher than in Fig. 2E. Carboxypeptidase A (CPA) was used as positive control. Antibodies against tyrosinated and detyrosinated EB1 were characterized in (*15*).

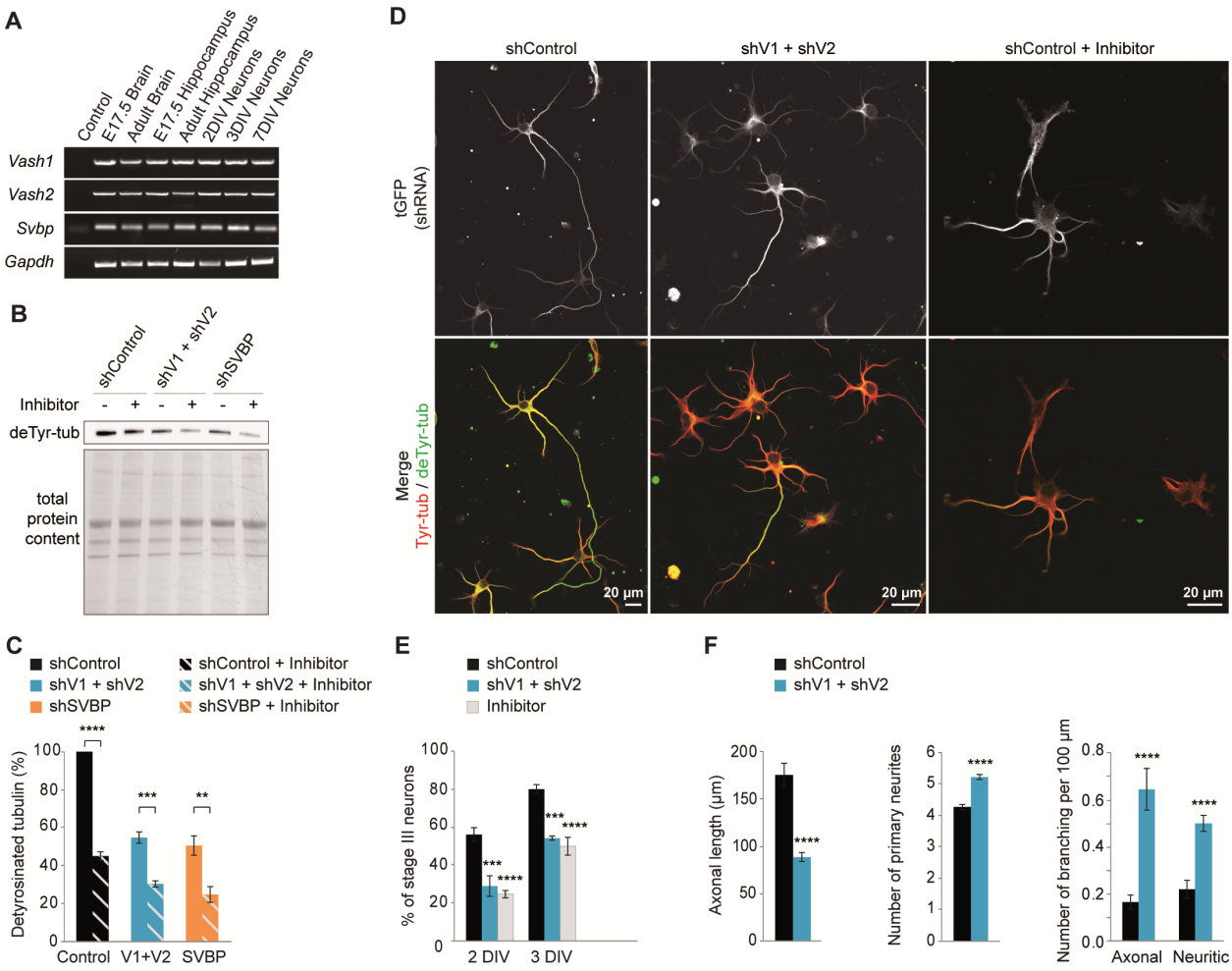

Fig. 3. Down-regulation of VASH1 and VASH2 affects neuronal differentiation. (**A**) *Vash1*, *Vash2* and *Svbp* transcripts are found in brain tissues and hippocampal neurons. RT-PCR reactions of 45 cycles were performed, except for *Gapdh* for which only 25 cycles were performed. (**B**) Immunoblot analysis of the effect of VASH1 and VASH2 (shV1 + shV2) or SVBP (shSVBP) down-regulation with or without alkyne-epoY (inhibitor) on detyrosinated α-tubulin levels in neurons. Neurons were transfected by electroporation with shRNAs associated to turboGFP (tGFP) cDNA just before plating and analyzed at 2DIV. Inhibitor (5 µM) was added at 0DIV and at 1DIV. Results from duplicate immunoblots of three independent neuronal cultures. (**C**) Quantification of immunoblots as in B (duplicate of 4 to 8 independent neuronal cultures). Results are expressed as percentage of detyrosinated tubulin related to shControl (mean ± SEM). Detyrosinated tubulin was significantly reduced in all conditions compared to shControl (One Way ANOVA with Sidak's

multiple comparisons test with **** p<0.0001). Detyrosinated tubulin was additionally reduced when shV1+shV2 and shSVBP transfected neurons were incubated with the inhibitor (Student t test). (**D-F**) Effect of vasohibins down-regulation on neurite outgrowth and axonal differentiation. Neurons were transfected as in B and analyzed by immunostaining at 2DIV and 3DIV. (**D**) Tyrosinated and detyrosinated α-tubulin levels were imaged at 2DIV using the same antibodies as in Fig. 2A. Levels of shRNA were imaged using an anti-tGFP antibody. Note that size of scale bars are different. (**E**) Stage III neurons (bearing an axon) were counted manually on immunofluorescence images (generated as in C) from 4 to 10 independent cultures, at 2DIV and 3DIV. Proportion of stage III neurons (an index of neuronal differentiation) is represented as mean ± SEM (One way ANOVA with Bonferroni multiple comparison test). (**F**) Morphometric analyses of at least 85 neurons (2DIV) using AutoNeuriteJ macro (see Materials and Methods for details) on immunofluorescence images generated as in D (mean ± SEM, Mann-Whitney tests). * p<0.05, ** p<0.01, *** p<0.001, **** p<0.0001.

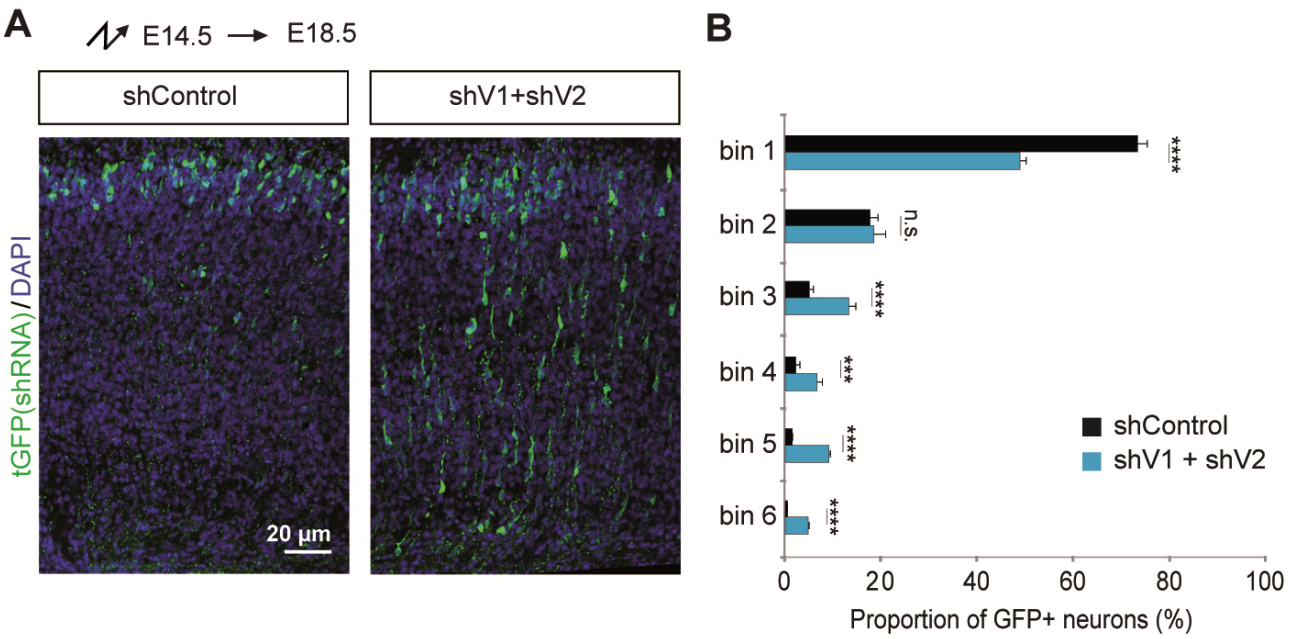

Fig. 4. Down-regulation of vasohibins affects radial migration of newborn cortical neurons. (**A**) Cortical coronal sections of E18.5 mice embryos electropored at E14.5 with indicated shRNAs. (**B**) Quantitative analysis showing the distribution of tGFP-positive neurons across the cortex divided into six bins of equal surface. Data from 5 brains per condition, 3 slides per embryo (at least 260 GFP^+-neurons per embryo), mean ± SEM. n.s., not significant, ***p<0.001, ****<0.0001 (Mann-Whitney test).

Supplementary Materials for

Vasohibins/SVBP are tubulin carboxypeptidases (TCP)

that regulate neuron differentiation

Chrystelle Aillaud, Christophe Bosc, Leticia Peris, Anouk Bosson, Pierre Heemeryck, Juliette Van Dijk, Julien Le Friec, Benoit Boulan, Frédérique Vossier, Laura E. Sanman, Salahuddin Syed, Neri Amara, Yohann Couté, Laurence Lafanechère, Eric Denarier, Christian Delphin, Laurent Pelletier, Sandrine Humbert, Matthew Bogyo, Annie Andrieux*, Krzysztof Rogowski*, and Marie-Jo Moutin*.

*correspondence to: moutinm@univ-grenoble-alpes.fr, annie.andrieux@univ-grenoble-alpes.fr, or krzysztof.rogowski@igh.cnrs.fr.

This PDF file includes:

Other Supplementary Materials for this manuscript includes the following:

Materials and Methods

Animals. Male or females mice were used between 2-4 months old. In accordance with the policy of the Institut des Neurosciences of Grenoble (GIN) and the French legislation, experiments were done in compliance with the European Community Council Directive of 24th November, 1986 (86/609/EEC). The research involving animals was authorized by the Direction Départementale de la protection des populations—Préfecture de l'Isère-France and by the ethics committee of GIN number 004 accredited by the French Ministry for of Research.

Preparation of tyrosinated tubulin and microtubule, and EB1. Bovine brain tubulin (12 mg/mL, prepared as in (*28*)) was tyrosinated by incubation for 45 min at 30°C with purified chicken TTL (1 mg/mL, gift from Steinmetz group) and 0.1 mM L-tyrosine or [^{14}C]-L-tyrosine (0.125 µCi/nmole) in 40 mM Pipes at pH 6.7, 60 mM KCl, 2.5 mM ATP, 1 mM DTT, 12.5 mM $MgCl_2$. Microtubules polymerization was allowed by one-third dilution in 100 mM PIPES at pH 6.7, 1 mM EGTA, 1 mM $MgCl_2$, 30% glycerol, 1 mM GTP and incubation at 32°C for 45 min, followed by another 45 min incubation with 50 µM Paclitaxel (Calbiochem). Microtubules were sedimented by 25 min centrifugation at 100,000 *g* and 30°C on 60% glycerol cushions. TTL-containing supernatant was discarded and tyrosinated-microtubules were resuspended in 100 mM PIPES at pH 6.7, 1 mM EGTA, 1 mM $MgCl_2$, 10% glycerol, 80 µM paclitaxel and stored at -20°C. To obtain unpolymerized tyrosinated-tubulin, paclitaxel was omitted during the whole procedure. EB1 was prepared as in (*28*).

TCP activity assays. In radioactivity tests using [^{14}C]-tyrosinated taxol-stabilized microtubule, enzyme activity was measured in 100 mM MES at pH 6.7, 1 mM EGTA and 1 mM $MgCl_2$ using 2 µM radiolabeled tubulin, except in Figs. 2D and S2D (quantity indicated in legend). Reactions were

performed for 45 min at 37°C (without or with previous incubation with inhibitors, see legends) and were stopped on ice by addition of 20 µg/ml bovine serum albumin and 10% perchloric acid and centrifugation. Tyrosine cleaved from microtubules was estimated by measuring radioactivity in the supernatant (a zero time control was subtracted). To compose the table of Fig. S1A, detyrosination activity from equal volumes of the various fractions was measured. In tests with inhibitors, detyrosination activity was tested after a 20 min preincubation with inhibitor (except in Figs. S2C and S2D where varying time of incubation were used as indicated in legend), and results with inhibitors were expressed as percentage of the activity in the control with corresponding solvent. In tests using immunoblots, enzyme activity was assayed with 5 µM substrates (taxol-stabilized microtubule, tubulin or EB1) in 100 mM MES at pH 6.7, 1 mM EGTA and 1 mM $MgCl_2$ for times indicated in figures. Positive controls were done with carboxypeptidase A (2 ng/mL). Reactions were stopped by addition of Laemmli buffer. A reaction with carboxypeptidase A (CPA), which efficiently cleaves aromatic and aliphatic C-terminal residues, was used as positive control. In tests using VASH/SVBP complexes purified on cobalt resin from HEK293T cells, enzymes concentration were approximated from in-gel Coomassie-blue staining of purified VASH1 and VASH2 together with standards of bovine serum albumin.

Enzyme enrichment. We designed a three-step purification procedure from brain lysate inspired from previous efforts (*23, 29*). All steps were carried out at 4°C. Adult mice brains were homogenized in 50 mM phosphate buffer at pH 6.7, 1 mM EGTA, 1 mM $MgCl_2$, 1 µg/ml DNAse with a protease inhibitor cocktail (cOmplete EDTA-free, Roche) and centrifuged 1 h at 100,000 *g*. The supernatant was collected (Fraction I). In step 1 (ammonium sulfate fractionation), Fraction I was slowly brought to 45% ammonium sulfate, incubated for 15 min and centrifuged 20 min at 15,000 *g*. Resulting supernatant underwent the same procedure at 65% ammonium sulfate. The pellet was re-suspended in one-eighth of initial volume with 50 mM MES pH 6.7, 1 mM EGTA, 1

mM $MgCl_2$ and desalted using Bio-Gel P30 (Bio-Rad) equilibrated with the same buffer (Fraction II). In step 2 (strong anion column), Fraction II was loaded onto a 5 mL Hitrap Q XL column (GE Healthcare) connected on a BioLogic DuoFlow chromatography systems (Biorad) and unbound proteins were collected (Fraction III). In step 3 (strong cation column): Fraction III adjusted to pH 6.2 and 0.12 M NaCl, was loaded on a 5mL Hitrap SP XL column (GE Heathcare). Proteins were eluted with a 0.12 M to 1 M NaCl gradient. Protein fractions were equilibrated in 50 mM MES at pH 6.7, 1 mM EGTA, 1 mM $MgCl_2$ (by desalting with BioGel P-30). TCP activity assay was performed on these fractions and activity containing fractions were pooled (Fraction IV). Purification data of a typical experiment are shown in Figs. 1A and S1A. For the quick enzyme enrichment (used in Fig. S1A, C, D), brain homogenate was directly proceeded to step 3, and then desalted.

Click chemistry (Cu-catalyzed azide-alkyne cycloaddition, CuCAAC reaction). Fraction IV was equilibrated in phosphate buffered solution at pH 7.4 and concentrated to 2 mg/ml. Following 1 h incubation at 37°C with 10 µM of alkyne-epoY or 10 µM of epoY (respectively clickable and control irreversible inhibitors, see structures in Fig. 1C, S2B), two equivalent volumes of azide-agarose beads (Jena Biosciences) were then added and click reaction was started by addition of 1 mM $CuSO_4$, 100 µM TBTA and 1 mM TCEP. Reaction was completed in 3 h at room temperature. For fluorescence labeling, 100 µM 5/6-TAMRA-PEG3-azide (Jena Bioscience) was used instead of azide-agarose beads.

Mass Spectrometry sample preparation. Removal of non-specifically bound proteins, and peptides preparation to be analyzed were achieved according to the Click Chemistry Capture Kit protocol (Jena Bioscience). Quickly, agarose-bound proteins were reduced and alkylated. Beads were washed with 1% SDS and 8 M urea. On-beads tryptic proteolysis (using Sequencing Grade

Modified Trypsin, Promega) was performed and released peptides were purified on C18 cartridges (Ultra-Micro spin columns, Harvard Apparatus).

Mass spectrometry-based proteomic analyses. Peptides were analyzed by nanoliquid chromatography coupled to tandem mass spectrometry (Ultimate 3000 coupled to LTQ-Orbitrap Velos Pro, Thermo Scientific) using a 120-min gradient as described in (*30*). Peptides and proteins were identified through concomitant searches against Uniprot (March 2017 version, *Mus musculus* taxonomy), classical contaminants (homemade) and the corresponding reversed databases using Mascot (version 2.5.1). The Proline software (http://proline.profiproteomics.fr) was used to filter the results (conservation of rank 1 peptides, peptide identification FDR < 1% as calculated on peptide scores by employing the reverse database strategy, and minimum of 1 specific peptide per identified protein group) before performing a compilation, grouping and comparison of the protein groups from the control and positive samples. Proteins from the contaminants database and additional keratins were discarded from the final list of identified proteins. Only proteins identified with a minimum of 3 specific spectral counts in the 3 replicates of positive samples and absent from the control samples were further considered.

Expression constructs. Mouse vasohibin-1 (VASH1) and vasohibin-2 (VASH2) cDNAs (accession numbers NM_177354 and NM_144879, respectively) were PCR-amplified and inserted into a home-made CAG promoter-containing vector, that generates proteins with a Flag tag at the N-terminus and with superfolder-GFP (sfGFP(*31*)) and a 6 His tag at the C-terminus (Flag-vasohibin-sfGFP-His). The corresponding control plasmid encodes Flag-sfGFP-His protein. Bicistronic plasmids allowing coupled expression of both vasohibins and SVBP were obtained by introducing, downstream of the Flag-vasohibin-sfGFP-His cDNA, a cassette containing the encephalomyocarditis virus IRES sequence followed by the cDNA encoding mouse SVBP

(accession number NM_024462) with a C-terminal Myc-tag (Flag-vasohibin-sfGFP-His/SVBP-Myc). Point mutations were introduced by PCR to generate enzymatically dead versions of vasohibins: C179A for VASH1 and C158A for VASH2, according to the numbering of accession numbers NP_796328 and NP_659128, respectively. The plasmid encoding mouse SVBP with C-terminal Myc and Flag tags (SVBP-Myc-Flag) was obtained from OriGene. Mouse *Eb1* cDNA (accession number NM_007896) was inserted into an EGFP-tagged vector in order to generate EB1-EGFP. Plasmid encoding His-EB1 for protein production in *E. coli* was described in (*15*). cDNAs coding for human tubulin α1B and mouse tubulin α8 (accession numbers NM_006082 and NM_017379, respectively) were PCR-amplified and inserted into a vector with N-terminal mCherry tag. Point mutations in α-tubulin cDNAs were introduced by PCR to replace the last aromatic residue by an alanine: Y451A for α1B-tubulin and F449A for α8-tubulin, according to the numbering of accession numbers NP_006073 and NP_059075, respectively. Plasmid expressing mouse-specific shRNAs were from OriGene: TL511800B for *Vash1*, TL506751C for *Vash2*, TL517601B for *Svbp* and TR30021 for control. For rescue experiment with SVBP, tGFP of the plasmid TL51701B containing the Svbp shRNA was extracted by digestion with Mlu I and Pme I and replaced by a cDNA encoding mouse *Svbp* with myc and FLAG epitopes at the C-terminus. The mutations G60A, G63A, T66C, G69A and G72A in the SVBP cDNA generate shRNA-resistance. All constructs were verified by DNA sequencing.

Purification of His-tagged vasohibins from HEK293T cells. HEK293T cells cotransfected with plasmids allowing expression of GFP or active/inactive forms of vasohibins and SVBP (Flag-sfGFP-His or Flag-(dead)VASH1/2-sfGFP-His and SVBP-Myc-Flag) were lysed in Tris buffer at pH 8.0, 0.5% TritonX100, 1 mM $MgCl_2$, 200 mM NaCl, 5 mM imidazole in the presence of protease inhibitor cocktail (cOmplete EDTA-free, Roche). After centrifugation (10 min at 16,000 *g* and 4°C), supernatants were collected and added onto 20 µL of cobalt resin (Sigma) and incubated

for 3 h at 4°C. After 3 washes with lysis buffer, proteins were eluted using 200 mM imidazole, Tris buffer at pH 8.0, 1 mM $MgCl_2$, 200 mM NaCl. Purified proteins were equilibrated by dialysis at 4°C in 100 mM Pipes, 1 mM EGTA and 1 mM $MgCl_2$ and directly used in radioactivity assays.

Cell culture and transfection. Hippocampal neurons and MEFs were prepared as previously described (*2*). HEK293T cells were maintained under standard conditions. HEK293T cells were transfected with JetPRIME transfection reagent (Polyplus-Transfection). MEFs and neurons were transfected using Amaxa Nucleofector kits (Lonza). A ratio of 1:1 was generally used for cDNA co-transfections (for VASH1/2 with SVBP, or for mCherry-tubulin with bicistronic plasmids allowing coupled expression of VASH1/2 and SVBP).

Antibodies, immuno-blotting and immune-fluorescence. Detyrosination activity was detected using antibodies specific for tyrosinated tubulin ($YL_{1/2}$, Tyr-tub) or native EB1 (Tyr-EB1), and C-terminally detyrosinated tubulin (deTyr-tub) or EB1 (deTyr-EB1). Control of total tubulin or EB1 was estimated with antibodies that recognizes both species (total α-tub or α3A1, total EB1 from BD Transduction lab.). All these antibodies were described and characterized in (*15*), except an anti-deTyr-tub that we recently developed (using the same peptide) in guinea pig which was used in immunofluorescence (1:1000, Fig. 3). The other primary antibodies were used as follow: mouse anti-His from Qiagen in immunofluorescence (1:5000), rabbit anti-Flag from Molecular Probes in immunofluorescence (1:10000), rabbit anti-GFP from Chromotek in immunoblot (1:5000), chicken anti-GFP from Millipore in immunofluorescence (1:500), rabbit anti-turboGFP from Invitrogen in immunofluorescence (1:1000) and in immunoblot (1:10000), mouse RFP antibody (for mCherry) from Sigma in immunoblot (1:2500), mouse anti-Tau from Millipore in immunofluorescence (1:500) and mouse anti-ankyrin G from SantaCruz in immunofluorescence (1:300).

For immunoblotting, cells were collected after 24 h of transfection. After washing with phosphate-buffered saline (PBS) medium at 37°C, cells were directly lysed in Laemmli buffer. Protein extracts were loaded on 10% acrylamide gels (Mini-PROTEAN® TGX Stain-Free™, Biorad) and transferred with Trans-Blot® Turbo (BioRad). Membranes were incubated with primary antibodies, with secondary antibodies conjugated with HRP (1:10 000, from Jackson ImmunoResearch), and finally revealed with Chemidoc camera (Biorad). For analysis and graphical representations of immunoblots (Fig. 3B,C and S6C), protein bands were quantified from triplicate blots of 3 different experiments using ImageJ software (National Institutes of Health, Bethesda, MD). Detyrosinated α-tubulin signal was normalized to the total protein content of the sample estimated from a stain-free gel image (the trihalo compounds in the Mini-PROTEAN® TGX Stain-Free™ gel react with tryptophan residues in proteins in a UV-induced 1-minute reaction to produce fluorescence).

For immunofluorescence, cells were generally fixed at 37°C in 4% paraformaldehyde, 4.2% sucrose, phosphate buffered saline medium (PBS) (except for ankyrin G staining for which methanol fixation at -20°C was used) and permeabilized using 0.1% Triton X-100, PBS. Cells were then incubated with primary antibodies, followed by incubation with secondary antibodies (see below) conjugated with either alexa-488, cyanine-3 or cyanine-5 fluorophores (1:1000). Nuclei were stained using Hoescht 33258 (1 μg/ml).

SDS-PAGE, immuno-blot or immunofluorescence data presented all over the manuscript are representative results from experiments performed at least 3-times.

RT-PCR and RT-qPCR amplifications. For RT-PCR, messenger RNAs from cells and tissues were prepared with the Dynabeads purification kit (Invitrogen). RT-PCR were performed with the Superscript One step RT-PCR System (Invitrogen) in 12.5 μL with 50 ng RNA. Products of respectively 697, 748 and 154 bp from mouse *Vash1*, *Vash2* and *Svbp* were amplified at 58°C by 45

cycles using the following primers: 5'-TACAAACCGCCCGCCTTCC and 5'-ACAGACCCTGACAGCTACCAACA for *Vash1*, 5'-GCAGCCTTCCATTGAGCGGT and 5'-CAGTCAACCCAGGGCTTTGCC for *Vash2*, 5'-CCAGCAGGAGCTGAAGCAAAGA and 5'-GCACCAGTTCCTCTGCCGGG for *Svbp*. *Gapdh* was amplified at 64°C by 25 cycles with 5'-TCAACGGGAAGCCCATCACCA and 5'-GTTTCTCCAGGCGGCACGTC primers. For RT-qPCR, cells were lysed using the SingleShot Cell Lysis kit (Bio-Rad) and analyzed using the iScript Reverse Transcription mix (Bio-Rad) and SsoAdvanced Universal SYBR Green Supermix (Bio-Rad). Products of 105 bp from mouse *Vash1*, *Vash2, Svbp* and *Gapdh* were amplified at 60°C by 40 cycles using the following primers: 5'-TGGCCAAGATCCACCCAGATG and 5'-TCGTCGGCTGGAAAGTAGGCAC for *Vash1,* 5'-AGGGGGAGAGATGGTAGGCGC and 5'-AGCCAGTCTGGGATCGTCATGG for *Vash2,* 5'-AACCAGCCTTCAGAGTGGAGAAGG and 5'-GCTCCGTCATGACTCTGTTGAGAGC for *Svbp,* and 5'-CGTGCCGCCTGGAGAAAC and 5'-TGGGAGTTGCTGTTGAAGTCG for *Gapdh*.

Morphometric neuron analysis. Mosaic images of 2DIV neuron fixed and stained with anti-tubulin antibody were acquired with a 20X N.A 0.5 objective on a DMI6000 Leica microscope with a motorized stand. Images were segmented after enhancement with a DoG filter. The cell bodies of single neurons were manually selected and used to process neurons individually with an homemade AutoNeuriteJ macro. Briefly the neuron images were skeletonized and neuritic loops were resolved using the "Analyze Skeleton 2D/3D ImageJ plugin"(*32*). The ends of neurites were marked using the "BinaryConnectivity" imageJ plugin (developed by G. Landini, http://www.mecourse.com/landinig/software/software.html). Images of each neurite from their ends to the cell body were produced. Among the neurites with a path overlap, the longest was defined as primary neurite. The images of primary neurites were substracted to images of overlapping neurites, thus defining secondary neurites and number of branching. Neurite lengths were measured. Neurites

with a length inferior to 12 µm were not considered in order to avoid skeletonization artifacts. An axon was defined among primary neurites of a single neuron if its length was at least 48 µm and 1.3-times longer than any other primary neurite. Using this macro we selected a minimum of 27 neurons for each condition and compared the mean axonal length, mean primary neurite number (excluding axon) and branching frequency.

In utero electroporation, tissue processing, immunohistochemistry and analyses. A full description is available in (*33*). Briefly, embryos from anesthetized timed-pregnant mice were electropored at E14.5 with plasmids allowing expression of shRNAs (see above). Four days later (E18.5), embryonic brains were dissected, fixed, cryosectioned and placed onto slides for analyses. Anti-tGFP primary antibodies (1:300) was incubated overnight at 4°C. Nuclei were counterstained with DAPI (Roche). Images were acquired with a 20X N.A 0.5 objective on a DMI6000 Leica microscope with a motorized stand and analyzed with Image J. The cortical region where transfected cells were detected was divided into 6 bins of equal surface in which GFP positive (GFP^+) neurons were counted (5 embryos per condition, 3 slides per embryo). At least 260 GFP^+ neurons were counted per embryo.

Syntheses and analytical characterization of designed TCP inhibitors. Synthesis steps, structure, molecular weight, ^1H and ^{13}C NMR and LC/MS analyses of epoY (**A**), alkyne-epoY (**B**), epoEY (**C**) and epoEEY (**D**).

A. epoY

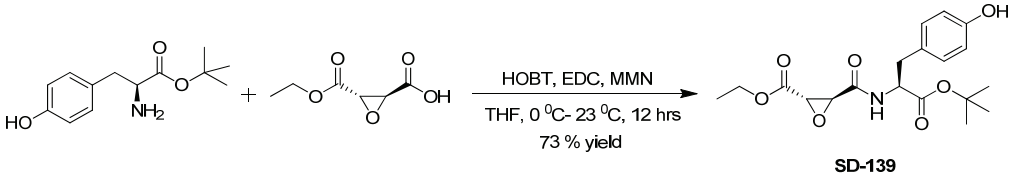

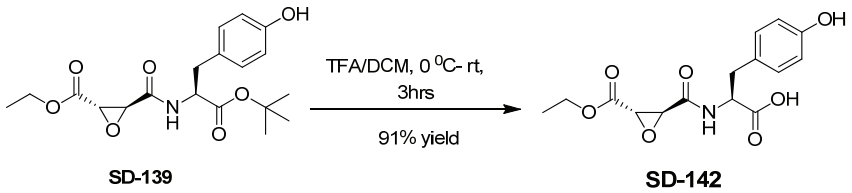

Synthesis of SD-139, (2S,3S)-ethyl 3-(S)-1-(tert-butoxy)-3- (4-hydroxyphenyl)-1-oxopropan-2-yl) carbamoyl)oxirane-2-carboxylate: To the solution of L-Tyrosine tert-butyl ester (118.6mg, 0.5 mmol), the 3-(ethoxycarbonyl) oxirane-2-carboxylic acid (80 mg, 0.5 mmole) and and *N*-methylmorpholine (87 mg, 0.75 mmol) in dry THF (10 mL) was added EDC (115 mg, 0.6 mmol) and HOBt (81 mg, 0.6 mmol) in portions at 0 ^{0}C. The reaction mixture was stirred at room temperature (rt) for 12 hours (hrs). After monitoring disappearance of starting material by LC-MS, the mixture was concentrated under reduced pressure. The concentrated residue was purified by flash column chromatography over silica gel with (eluent: 2-10 % of MeOH in DCM) to afford **SD-139** as a colorless solid (138 mg, 73 %).

Synthesis of epoY (SD-142), (S)-2-((2S,3S)-3-(ethoxycarbonyl) oxirane -2-carboxamido)-3-(4-hydroxyphenyl) propanoic acid: The t-Butyl group was removed by incubation with 30% TFA/DCM(v/v) for 2 hrs. The progress of reaction was monitored by LC-MS. After completion of reaction, the solvent was evaporated under vacuum and the product was then co-evaporated with toluene to afford **epoY (SD-142)** as a colorless solid (90 mg, 91 %).

^{1}H NMR (400 MHz, Chloroform-d) δ 6.94 (d, *J* = 8.4 Hz, 2H), 6.77 – 6.72 (m, 2H), 4.75 (q, *J* = 5.7 Hz, 1H), 4.28 – 4.19 (m, 2H), 3.61 (dd, *J* = 1.9, 0.6 Hz, 1H), 3.22 – 3.15 (m, 2H), 3.00 (dd, *J* = 14.1, 6.3 Hz, 1H), 1.30 (t, *J* = 7.2 Hz, 3H). ^{13}C NMR (101 MHz, cdcl$_3$) δ 176.92, 171.38, 166.78, 130.21, 126.53, 115.39, 62.33, 53.63, 52.67, 52.58, 36.34, 13.88. MS (ESI) m/z: calcd: $[M+H]^+$ 324.1, measured: $[M+H]^+$ 324.09

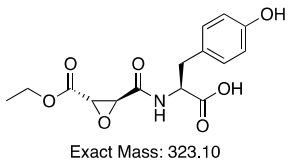

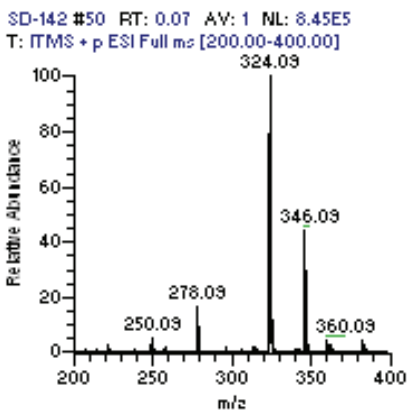

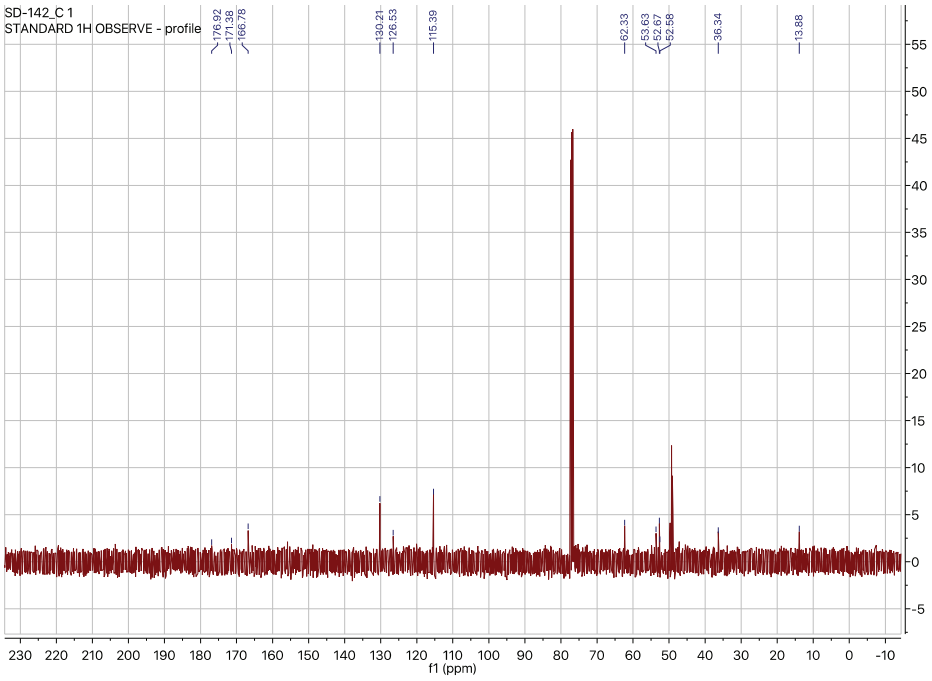

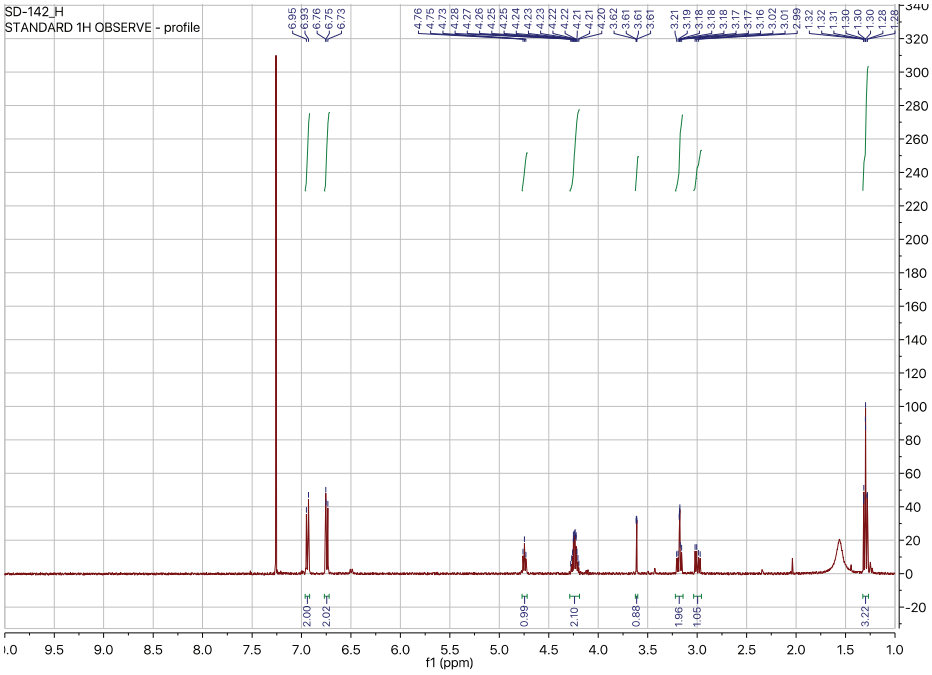

B. alkyne-epoY

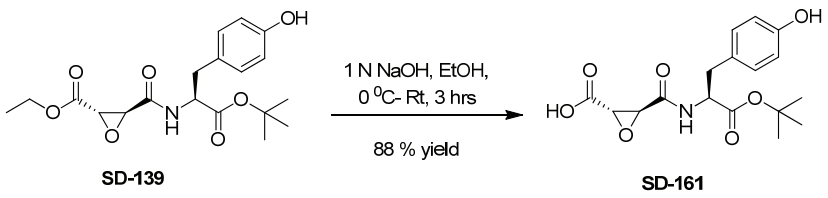

SD-139 **SD-161**

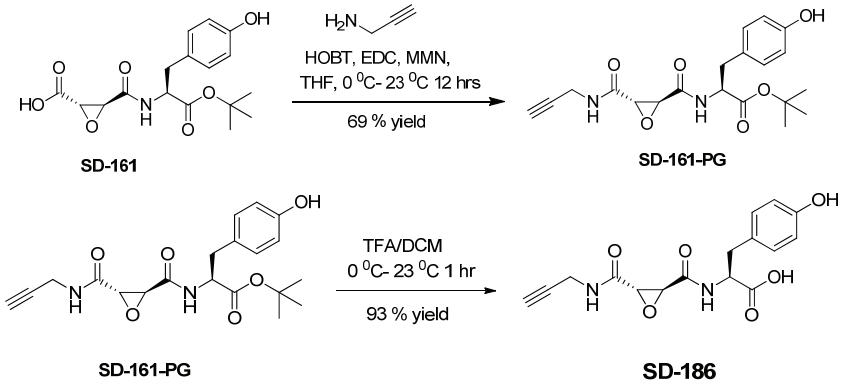

Synthesis of SD-161 **(2S,3S)-3-(S)-1-(tert-butoxy)-3-(4-hydroxyphenyl)-1-oxopropan-2-yl)carbamoyl)oxirane-2-carboxylic acid**: to an ice cooled solution of SD-139 (75 mg, 0.2 mmol) in ethanol (2 mL) was added drop wise a solution of potassium hydroxide (13 mg, 0.24 mmol) in ethanol (1 mL) over 15 min. After this addition the reaction mixture was allowed to stir in ice for 1 hour. The cooling bath was then removed and the reaction mixture was stirred for further 2 hrs at room temperature. Afterwards the ethanol was removed under reduced pressure leaving an off white solid. This salt was then taken up with 5 mL of water and washed three times with dichloride methane. The aqueous phase was acidified by addition of concentrated hydrochloric acid to pH 3.0 and extracted four times with ethyl acetate. The combined organic phase was dried over magnesium sulphate and concentrated under reduced pressure. After freeze drying the pure product was obtained as a colorless solid (62 mg, 88% yield).

Synthesis of SD-161-PG **(S)-tert-butyl 3-(4-hydroxyphenyl)-2-((2S,3S)-3-(prop-2-yn-1-ylcarbamoyl)oxirane-2-carboxamido) propanoate:** To the solution acid SD-161 (60 mg, 0.17 mmol), the propargylamine (10 mg, 0.17 mmole) and and *N*-methylmorpholine (20 mg, 0.25 mmol) in dry THF (5 mL) was added EDC (191.7 mg, 0.20 mmol) and HOBt (27 mg, 0.20 mmol) in portions at 0 ^{0}C. The reaction mixture was stirred at room temperature for 12 h. After monitoring disappearance of starting material by LC-MS, the mixture was concentrated under reduced pressure. The concentrated residue was purified by flash column chromatography over silica gel with (eluent : 2-10 % of MeOH in DCM) to afford **SD-161-PG** as a colorless gum like solid (46 mg, 69 %).

<u>Synthesis of Alkyne-epoY (SD-186)</u> (S)-3-(4-hydroxyphenyl)-2-((2S,3S)-3-(prop-2-yn-1-ylcarbamoyl) oxirane-2-carboxamido) propanoic acid: The t-Butyl group was removed by incubation with 30% TFA/DCM (v/v) for 2 hrs at room temperature. The progress of reaction was monitored by LC-MS. After completion of reaction, the solvent was evaporated under vacuum and the product was then co-evaporated with toluene to afford **Alkyne-epoY** (**SD-186)** as a colorless solid (31 mg, 93 %).

^{1}H NMR (400 MHz, Chloroform-d) δ 6.91 – 6.86 (m, 2H), 6.72 – 6.66 (m, 2H), 4.64 (ddd, *J* = 6.7, 5.5, 3.1 Hz, 1H), 3.94 (dd, *J* = 2.6, 0.8 Hz, 1H), 3.43 (d, *J* = 2.0 Hz, 1H), 3.17 – 3.08 (m, 2H), 2.94 – 2.88 (m, 1H), 2.21 (t, *J* = 2.6 Hz, 1H). ^{13}C NMR (101 MHz, cdcl$_3$) δ 172.80, 166.86, 166.05, 155.80, 130.20, 126.60, 115.43, 78.37, 71.73, 54.06, 53.98, 52.72, 36.20, 28.65. MS (ESI) m/z: calcd: $[M+H]^+$ 333.1, measured: $[M+Na]^+$ 355.18

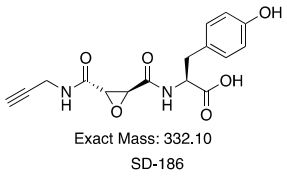

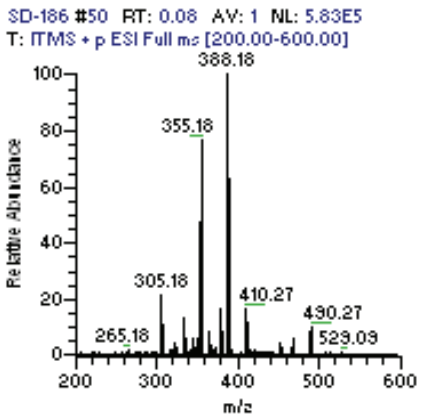

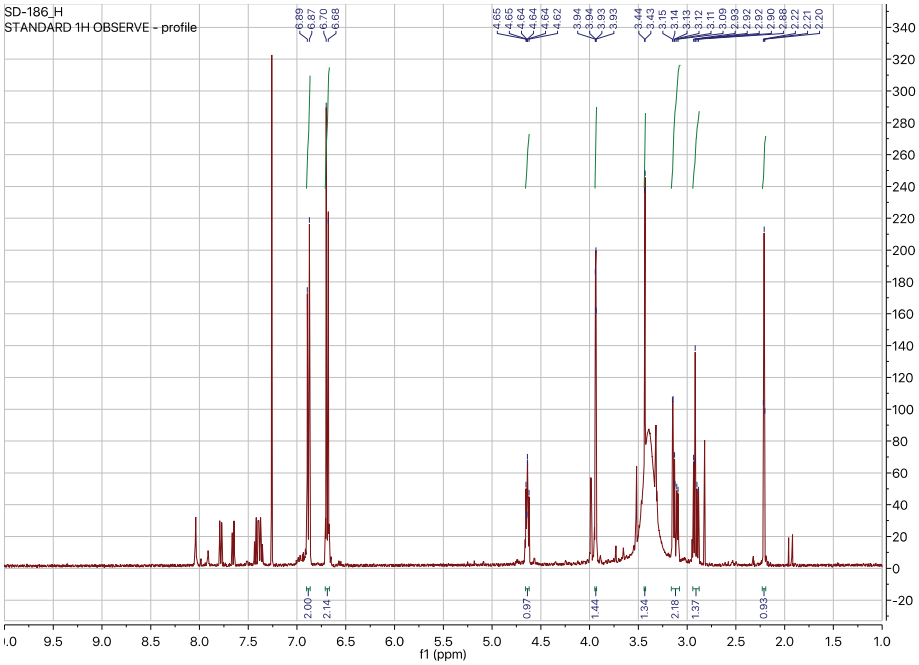

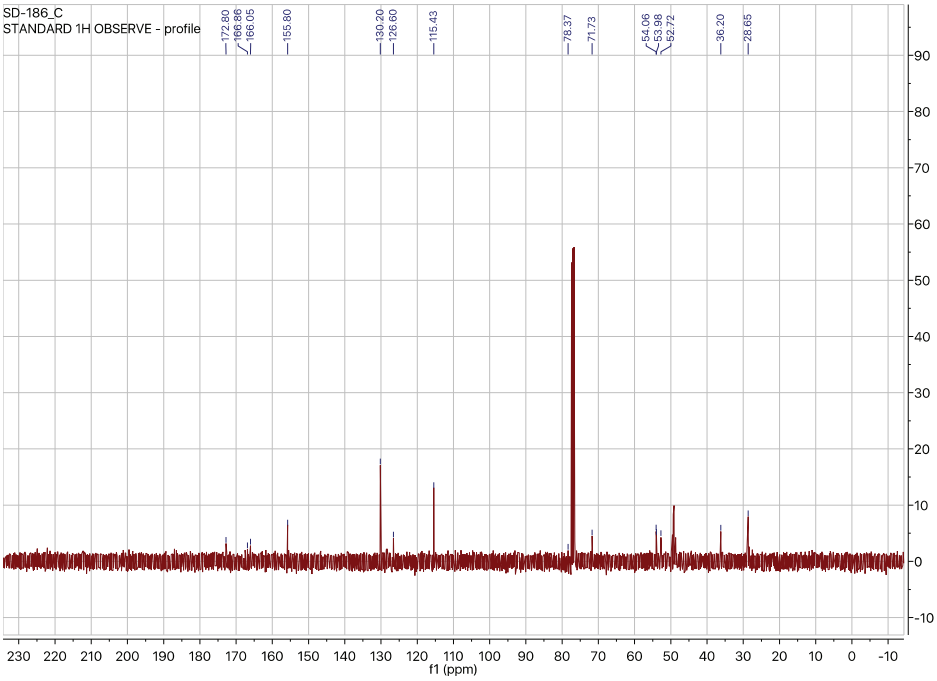

C. epoEY

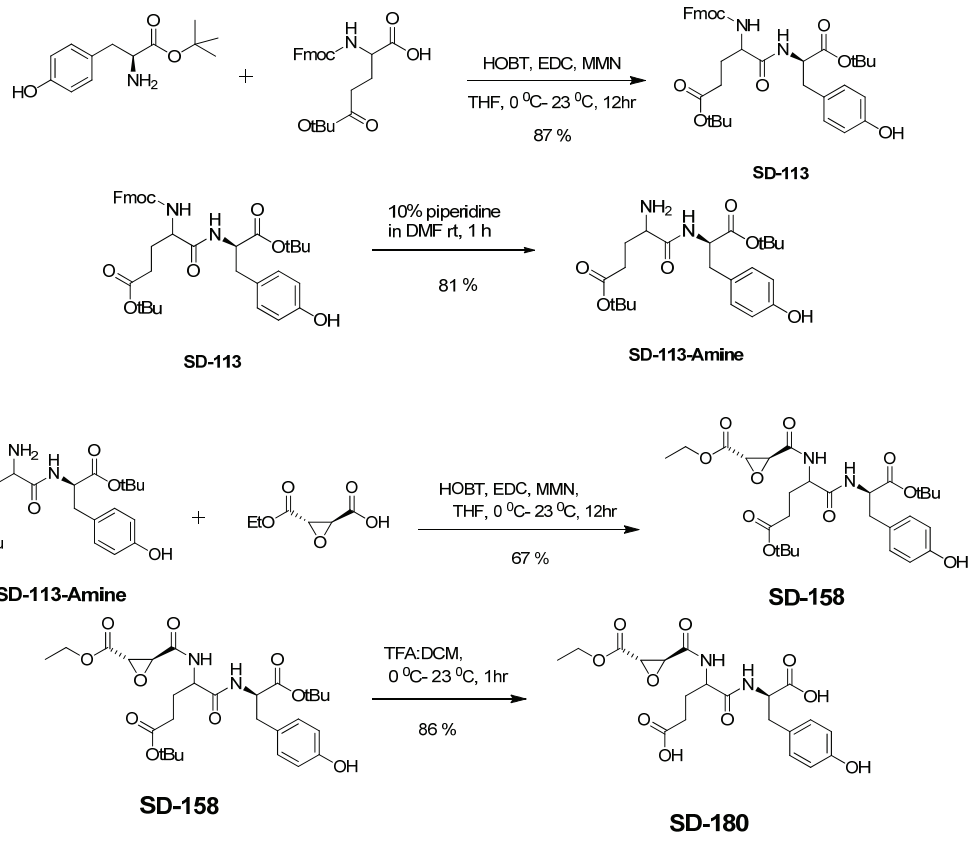

<u>Synthesis of SD-139</u> (2S,3S)-ethyl 3-(S)-1-(tert-butoxy)-3- (4-hydroxyphenyl)-1-oxopropan-2-yl) carbamoyl)oxirane-2-carboxylate: To the solution of L-Tyrosine tert-butyl ester (237.2 mg, 1

mmol), the Fmoc-Glu(OtBu)-OH (425 mg, 1 mmole) and and *N*-methylmorpholine (175 mg , 1.5 mmol) in dry THF (15 mL) was added EDC (229 mg, 1.2 mmol) and HOBt (162 mg, 1.2 mmol) in portions at 0 ^{0}C. The reaction mixture was stirred at room temperature for 12 h. After monitoring disappearance of starting material by LC-MS, the mixture was concentrated under reduced pressure. The concentrated residue was purified by flash column chromatography over silica gel with (eluent: 1-10 % of MeOH in DCM) to afford **SD-157** as a colorless solid (560 mg, 87 %).

Synthesis of SD-113-Amine **tert-butyl 4-amino-5-(R)-1-(tert-butoxy)-3-(4-hydroxyphenyl) -1-oxopropan-2-yl)amino)-5-oxopentanoate**: The Fmoc of **SD-113** was removed with 20% piperidine/DMF (v/v) for 30 min. The progress of reaction was monitored by LC-MS. After completion of reaction, the solvent was evaporated under vacuum and the crude mixture was purified by flash column chromatography over silica gel with (eluent: 1-10 % of MeOH in DCM with drop of TEA) to afford **SD-113_Amine** as a colorless solid (171 mg, 81 %).

Synthesis of SD-158: **(2S,3S)-ethyl 3-((5-(tert-butoxy)-1-(((R)-1-(tert-butoxy)-3-(4-hydroxyphenyl)-1-oxopropan-2-yl)amino)-1,5-dioxopentan-2-yl)carbamoyl) oxirane-2-carboxylate.** Compound **SD-158** was synthesized from **SD-113-Amine** (150 mg, 0.35 mmol) by following the same procedure described for the synthesis of **SD-139** to afford **SD-158** as white solid (132 mg, 67%).

Synthesis of epoEY (SD-180): Compound SD-180 was synthesized from SD-158 (50 mg, 0.08 mmol) by following the same standard procedure described for the *t*-Butyl deprotection in the synthesis of SD-142 to afford **epoEY** (**SD-180)** as white solid (31 mg, 86%).

^{1}H NMR (400 MHz, Chloroform-d) δ 6.94 – 6.87 (m, 2H), 6.65 (d, *J* = 8.1 Hz, 2H), 4.62 (t, *J* = 6.3 Hz, 1H), 4.35 (d, *J* = 7.0 Hz, 1H), 4.19 (qt, *J* = 7.8, 4.0 Hz, 2H), 3.53 (dd, *J* = 22.0, 1.7 Hz, 2H), 3.06 (dd, *J* = 14.2, 5.2 Hz, 1H), 2.89 – 2.82 (m, 0H), 2.32 – 2.21 (m, 2H), 2.01 – 1.90 (m, 1H), 1.80 (dd, *J* = 14.5, 7.7 Hz, 1H), 1.25 (t, *J* = 7.1 Hz, 3H). 13C NMR (101 MHz, cdcl3) δ 178.15, 174.41,

173.76, 167.22, 163.08, 155.63, 130.26, 126.90, 115.23, 62.43, 53.51, 52.44, 51.93, 36.64, 36.37, 31.46, 27.06, 13.80. MS (ESI) m/z: calcd: $[M+H]^+$ 453.14, measured: $[M+H]^+$ 453.18

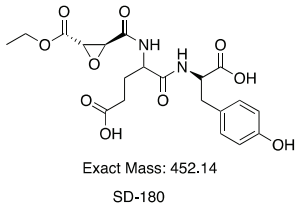

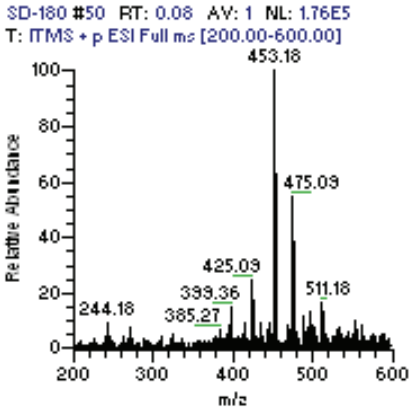

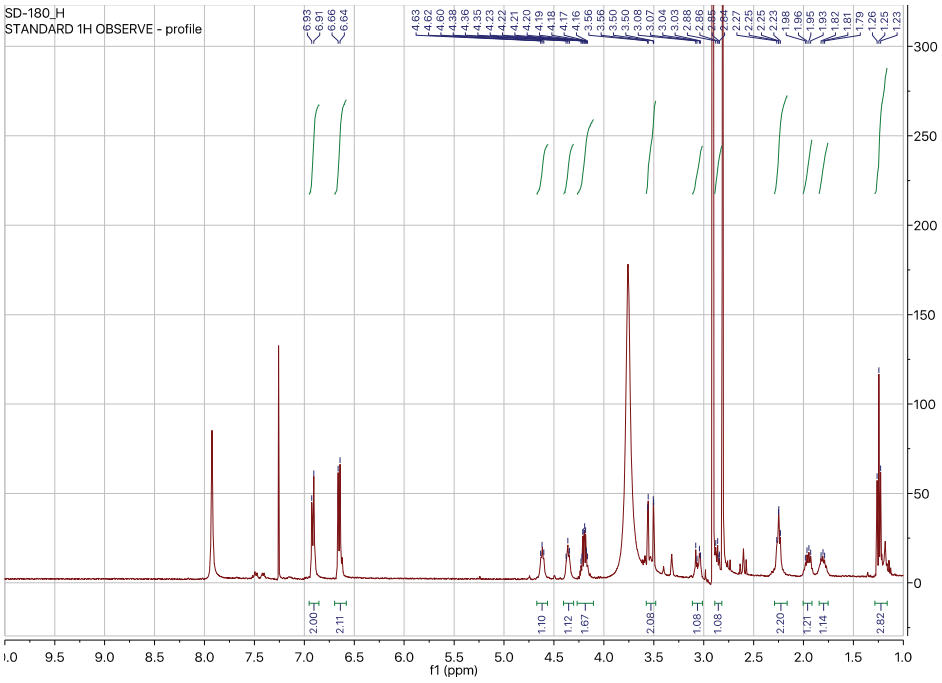

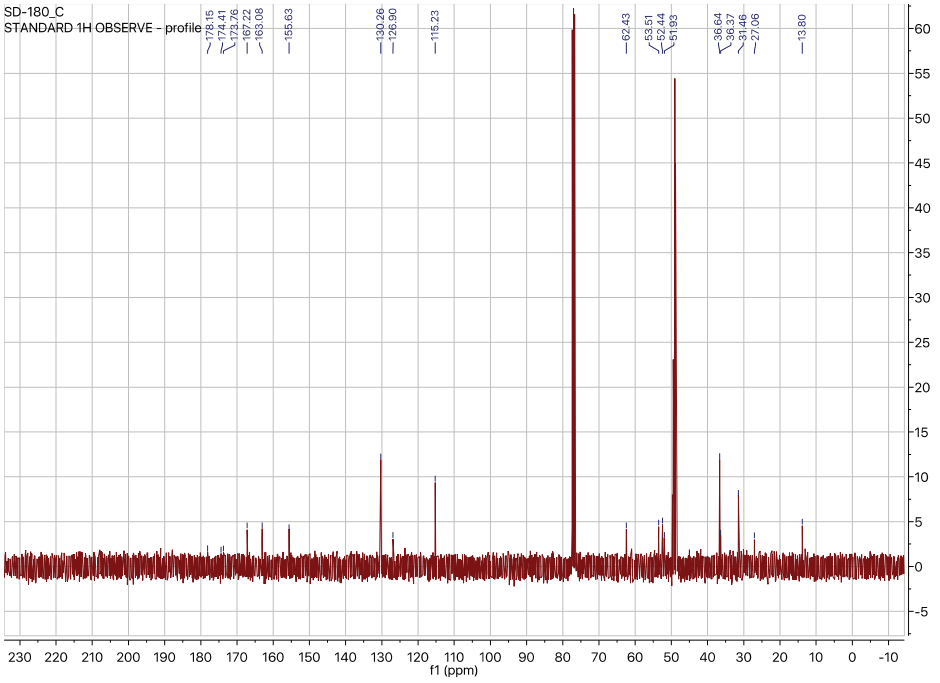

D. epoEEY

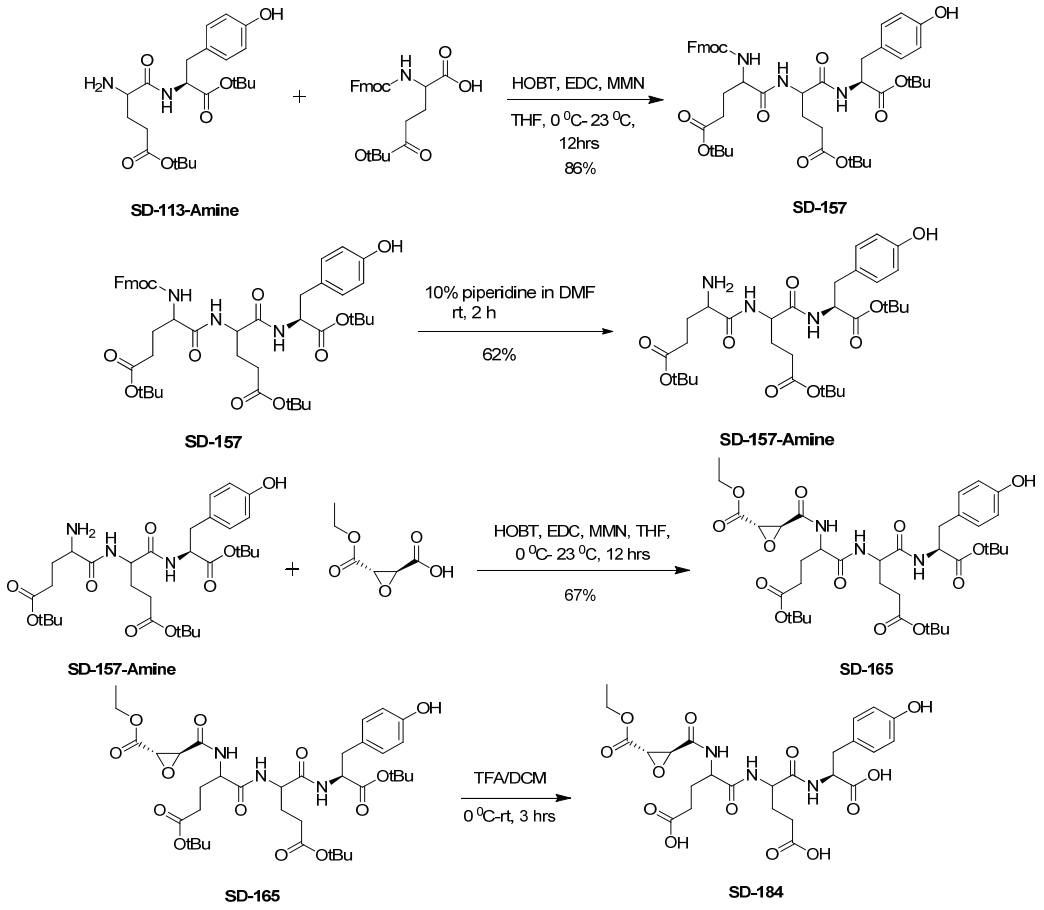

<u>Synthesis of SD-157</u> tert-butyl 5,8-bis(3-(tert-butoxy)-3-oxopropyl)-1-(9H-fluoren-9-yl)-11-(4-hydroxybenzyl)-3,6,9-trioxo-2-oxa-4,7,10-triazadodecan-12-oate: To the solution of SD-113-Amine (211 mg, 0.5 mmol), the Fmoc-Glu(OtBu)-OH (212 mg, 0.5 mmole) and *N*-methylmorpholine (87 mg, 0.75 mmol) in dry THF (10 mL) was added EDC (115 mg, 0.6 mmol) and HOBt (81 mg, 0.6 mmol) in portions at 0 ^{0}C. The reaction mixture was stirred at room temperature for 12 h. After monitoring disappearance of starting material by LC-MS, the mixture was concentrated under reduced pressure. The concentrated residue was purified by flash column chromatography over silica gel with (eluent: 1-10 % of MeOH in DCM) to afford **SD-157** as a colorless solid (289 mg, 69 %).

<u>Synthesis of SD-157-Amine</u> tert-butyl 4-amino-5-((5-(tert-butoxy)-1-(S)-1-(tert-butoxy)-3-(4-hydroxyphenyl)-1-oxopropan-2-yl)amino)-1,5-dioxopentan-2-yl)amino)-5-oxopentanoate: The Fmoc of **SD-157** was removed with 20% piperidine/DMF (v/v) for 30 min. The progress of reaction

was monitored by LC-MS. After completion of reaction, the solvent was evaporated under vacuum and the crude mixture was purified by flash column chromatography over silica gel with (eluent: 1-10 % of MeOH in DCM with drop of TEA) to afford **SD-157-Amine** as a colorless solid (90 mg, 62 %).

Synthesis of SD-165 **(2S,3S)-ethyl 3-(((5S)-8-(3-(tert-butoxy)-3-oxopropyl)-5-(4-hydroxybenzyl)-2,2,16,16-tetramethyl-4,7,10,14-tetraoxo-3,15-dioxa-6,9-diazaheptadecan-11-yl)carbamoyl)oxirane-2-carboxylate:** Compound SD-**165** was synthesized from **SD-157**-Amine (90 mg, 0.14 mmol) by following the same procedure described for the synthesis of **SD-139** to afford **SD-165** as white solid (70 mg, 67%).

Synthesis of epoEEY (SD-184) **5-((4-carboxy-1-(((S)-1-carboxy-2-(4-hydroxyphenyl)ethyl)amino)-1-oxobutan-2-yl)amino)-4-((2S,3S)-3-(ethoxycarbonyl)oxirane-2-carboxamido)-5-oxopentanoic acid:** The t-Butyl groups of SD-165 was removed by incubation with 30% TFA/DCM(v/v) for 2hrs. The progress of reaction was monitored by LC-MS. After completion of reaction, the solvent was evaporated under vacuum and the product was then co-evaporated with toluene to afford epoEEY (**SD-184)** as a colorless solid (35 mg, 91 %).

^{1}H NMR (400 MHz, Methanol-d4) δ 7.04 (d, *J* = 8.4 Hz, 2H), 6.73 – 6.64 (m, 2H), 4.61 – 4.52 (m, 1H), 4.39 (dt, *J* = 8.8, 5.7 Hz, 2H), 4.25 (qd, *J* = 7.1, 1.9 Hz, 1H), 4.31 – 4.06 (m, 1H), 3.65 (ddd, *J* = 18.3, 1.8, 0.6 Hz, 2H), 3.09 (dd, *J* = 14.1, 5.3 Hz, 1H), 2.92 (dd, *J* = 14.1, 8.0 Hz, 1H), 2.45 – 2.29 (m, 4H), 2.13 – 1.99 (m, 1H), 1.98 – 1.83 (m, 2H), 1.32 – 1.20 (m, 3H). ^{13}C NMR (101 MHz, cd_3od) δ 175.11, 169.03, 162.65, 162.40, 157.68, 155.86, 129.92, 127.37, 114.85, 61.77, 58.89, 53.85, 52.70, 51.77, 39.34, 36.15, 26.67, 12.94. MS (ESI) m/z: calcd: $[M+H]^+$ 582.19, measured: $[M+H]^+$ 582.18

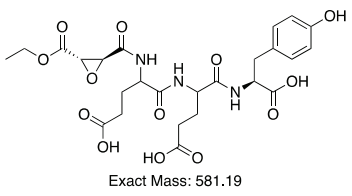

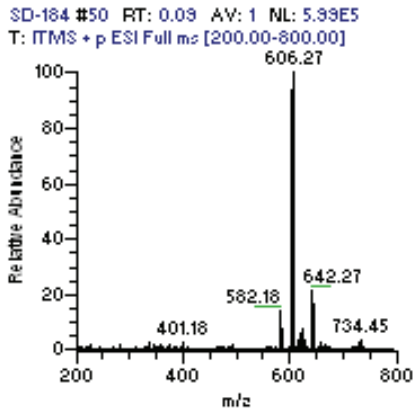

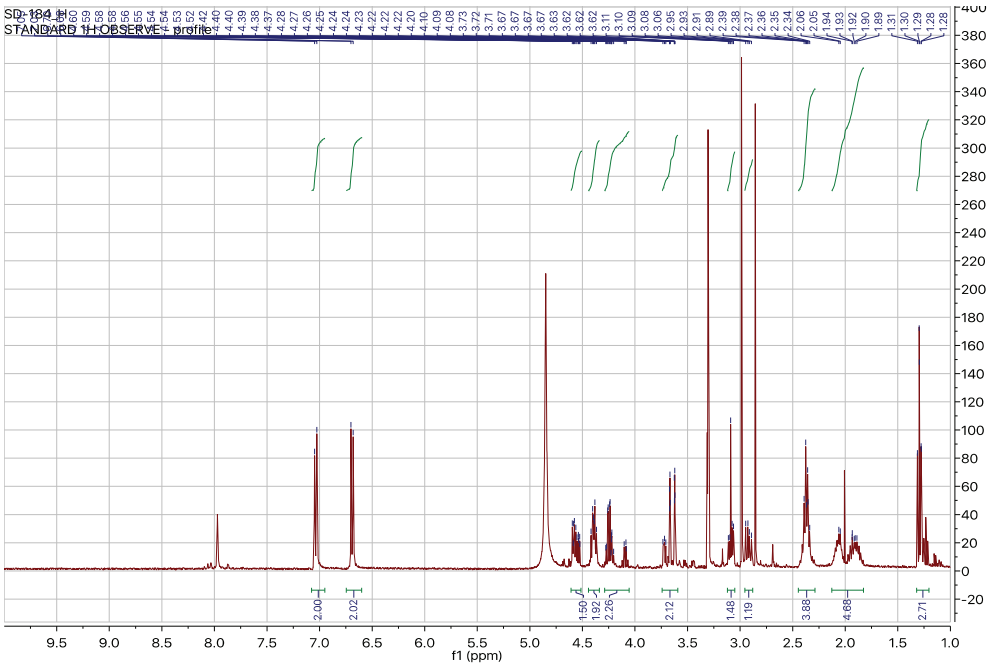
SD-184_H
STANDARD 1H OBSERVE - profile
f1 (ppm)

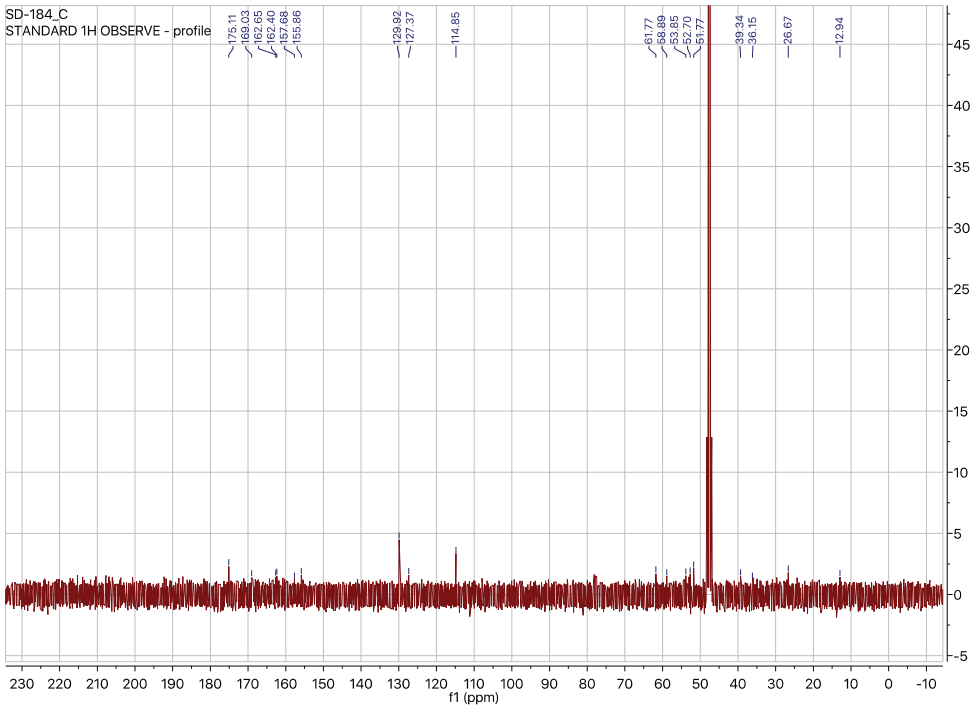
SD-184_C
STANDARD 1H OBSERVE - profile
175.11
169.03
162.65
162.40
155.88
155.68
129.92
127.37
114.85
61.77
59.69
53.85
52.70
51.77
39.34
36.15
26.67
12.94
f1 (ppm)

Authors Contributions

CA performed all biochemistry experiments (Figs 1, 2, S1-S4) and succeeded to identify brain TCP. AB initially developed TCP enzyme enrichment steps and TCP activity assays. KR and JVD originally designed and developed the method for using the C-terminal amino acid sequence of α-tubulin for inhibition of TCPase activity. KR and JVD initially considered TCP enzymes as having reactive cysteine(s) and performed functional characterization of peptide based inhibitors. MB designed the covalent inhibitors used to purify brain TCP. SS and NA synthesized and performed analytical characterization of the TCP inhibitors. LS together with CA worked out labeling and purification methods using the covalent inhibitors. YC performed the mass spectrometry-based proteomic analyses. CB engineered all DNA constructs and prepared all the figures. LaP performed RT-qPCR experiments. LeP, PH and MJM performed the experiments with neurons, LeP analyzed them assisted by PH, and LeP performed the statistical analyses. ED and BB developed AutoNeuriteJ macro used for neuron morphometric analysis. JLF electropored mouse embryos and CA quantified cortical neurons migration. FV assisted everybody for plasmids amplifications and basic biochemistry. MJM oversaw the entire project and assisted with data interpretation. AA, CB, CD, LL and SH provide intellectual inputs to the project. CA, MJM and MB wrote the manuscript with the contribution of all co-authors.

A

Fraction	Purification step	Volume (ml)	Protein amount (mg)	Total activity (µmole)	Specific activity (µmole/mg)	Purification (fold)	Yield (%)
I	Brain homogenate	70	338.56	1.41	0.004	-	100
II	Ammonium Sulfate	7	39.35	3.77	0.096	23	267
III	Q sepharose	20	15.03	3.17	0.211	51	225
IV	SP sepharose	6	0.09	0.14	1.533	368	10

B

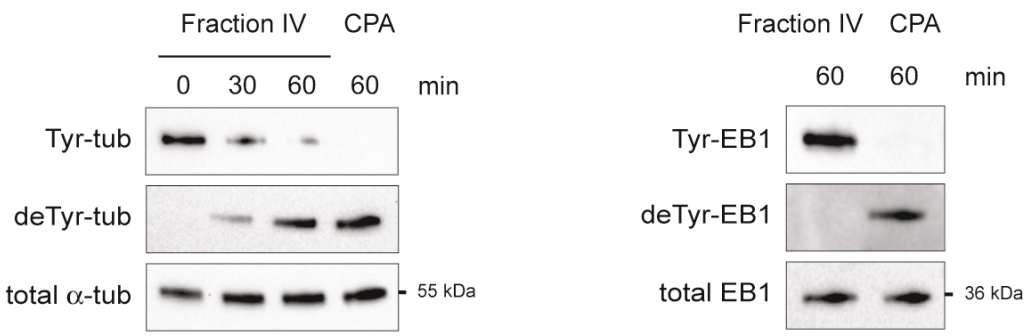

Fig. S1. TCP enriched fraction prefers tubulin as substrate. (A) Table of enzyme enrichment steps from mouse brain tissue. Detyrosination activity from equal volumes of the various fractions was estimated by measuring tyrosine released from [^{14}C]-tyrosine labeled microtubules (2 µM) after 45 min incubation. **(B)** Detyrosination of tubulin and EB1 (5 µM) by fraction IV revealed by immunoblot. A reaction with carboxypeptidase A (CPA) was used as positive control.

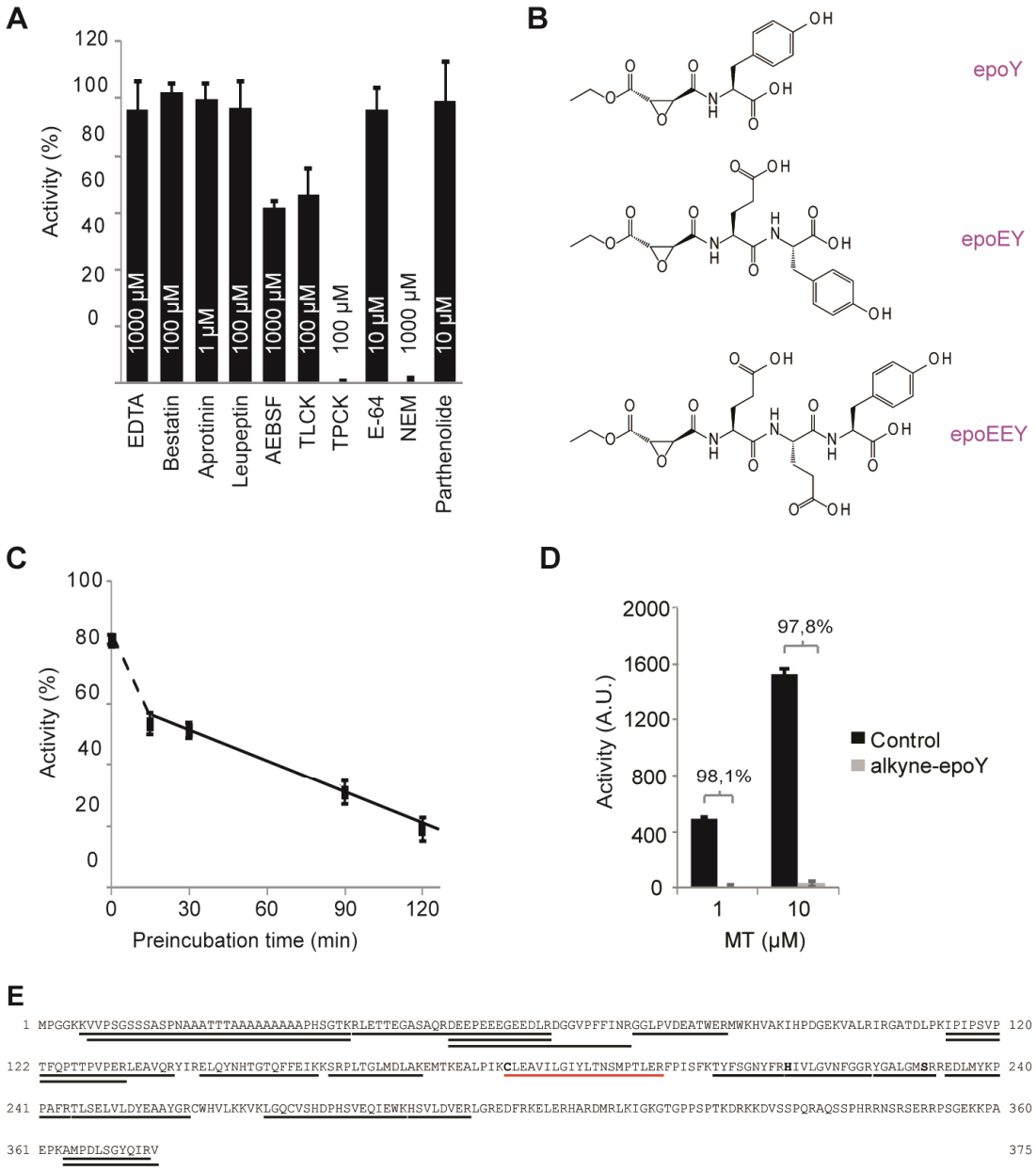

Fig. S2. Inhibition and identification of mouse brain TCP. (A) Screening of proteases inhibitor potencies on the activity of the enzyme-enriched fraction prepared by the quick enrichment protocol. Inhibitors were used at the supplier's highest advised concentration. Results with inhibitors are expressed as percentage of the activity in the control (mean ± SD, n = 3-5). (**B**) Structure of designed inhibitors, EpoY, epoEY and epoEEY. **(C)** Time-dependent inhibition of putative TCP by alkyne-epoY. Fraction IV was preincubated with 1 µM alkyne-epoY and detyrosination activity was tested as in A. Results are expressed as the percentage of activity in the control (mean ± SD, n = 3). Increasing the time of pre-incubation with alkyne-epoY enhanced its inhibitory effect, indicative of a covalent reaction between inhibitor and putative TCP. **(D)** Effect of substrate concentration on alkyne-epoY inhibition. Fraction IV was preincubated 3h with 1 µM inhibitor or DMSO (control) before activity measurement on radiolabeled microtubules. Results are expressed as the mean ± SD (n = 3). Increasing levels of microtubules by 10-fold did not restore the tyrosine cleavage activity of inhibited Fraction IV. **(E)** Sequence of mouse vasohibin-1 (VASH1) with all the peptides (underlined in black) identified by mass spectrometry of three independent purifications. The putative catalytic triad

residues are in bold. No vasohibin-1 peptide was found in the three control experiments done with epoY which is not clickable. No peptide carrying the catalytic Cys179 (underlined in red) was identified due to its covalent binding to inhibitor and agarose beads.

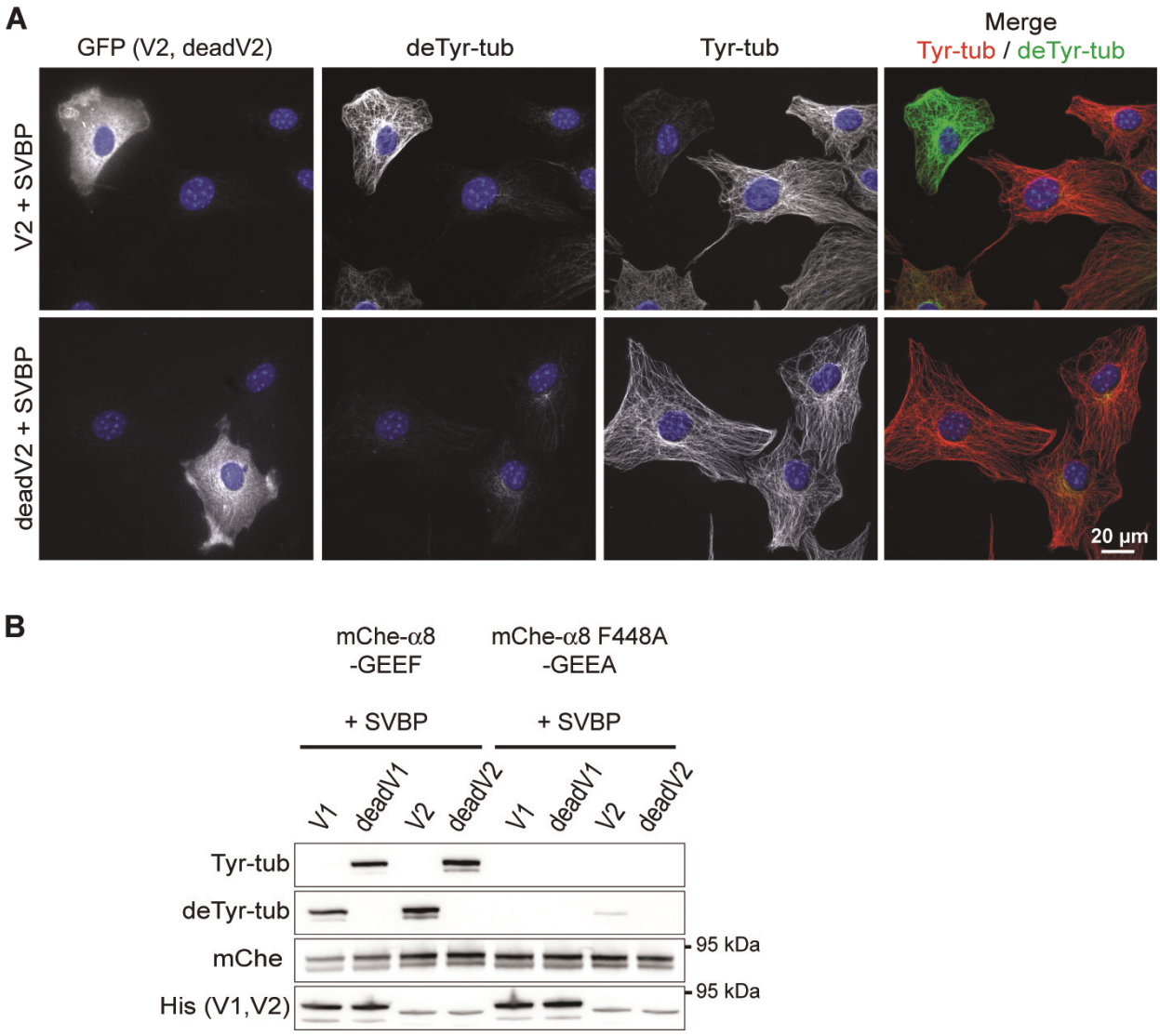

Fig. S3. VASH1 and VASH2 associated to SVBP are potent tubulin Tyr/Phe carboxypeptidases. (**A**) Immunofluorescence analysis of de/tyrosinated α-tubulin pools from MEF cells cotransfected with plasmids encoding active or inactive VASH2 and SVBP (V2 or deadV2, respectively). Carboxypeptidase activity was revealed by immunofluorescence with the same antibodies as in Fig. 2B. Vasohibins were probed with anti-GFP antibody. (**B**) Immunoblot of protein extracts from HEK293T cells expressing mCherry-α8-tubulin, each VASH and SVBP. Native or mutated versions of α8-tubulin, respectively ending with GEEF or GEEA, were used. Levels of de/tyrosinated tubulin were measured as in Fig. 2A. Antibody to mCherry demonstrates same amounts of exogenous α-tubulin.

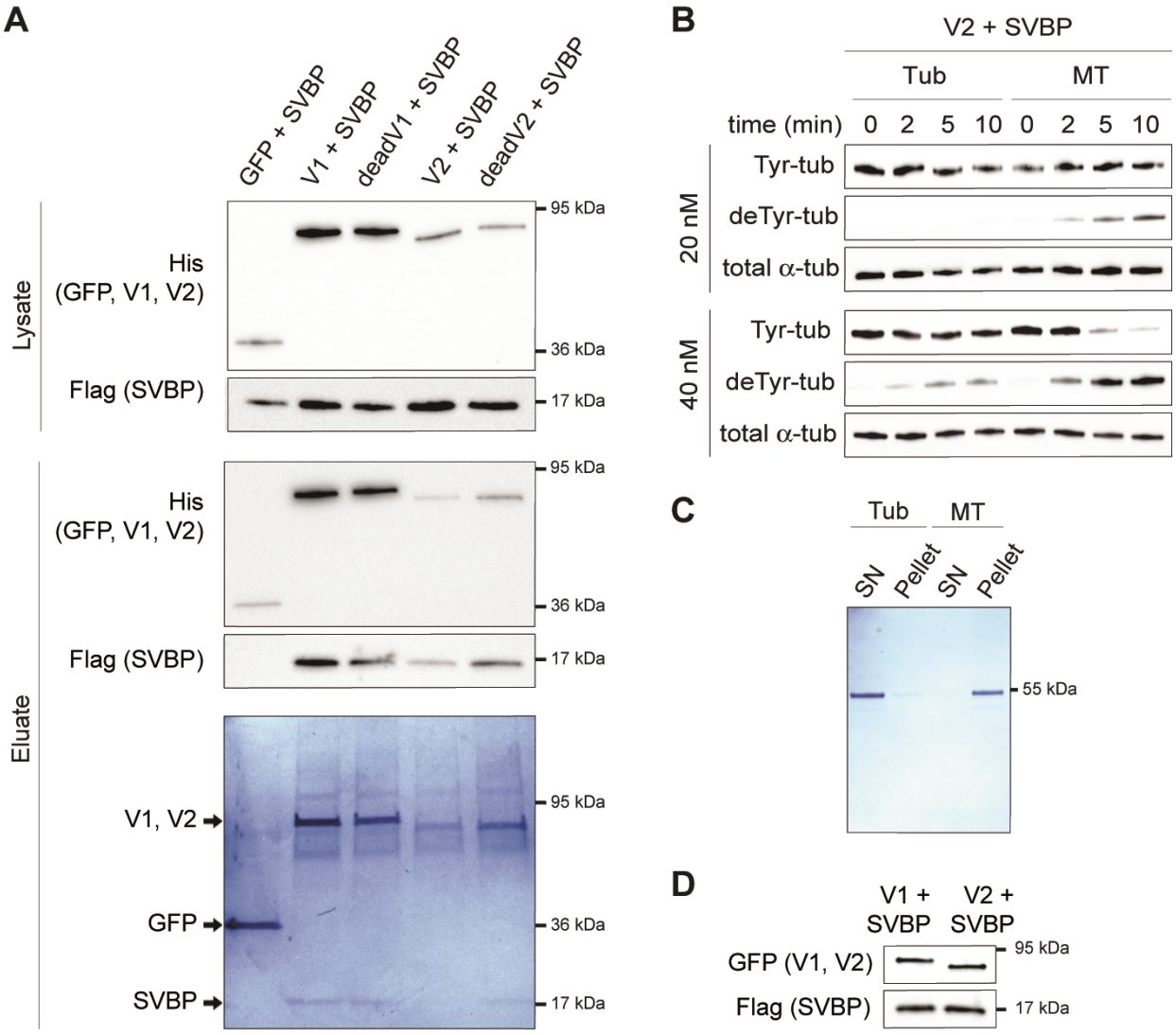

Fig. S4. Purification and properties of VASH/SVBP complexes. (A) Immunoblot analysis (upper panels) and SDS-PAGE (lower panel) of the purification of vasohibin/SVBP complexes. Vasohibins and their catalytic dead versions were co-expressed with SVBP in HEK293T cells as in Fig. 2A and then purified on cobalt resin. A GFP construct (bearing an His-tag) was used as control. GFP and vasohibins were probed with anti-His antibody, and SVBP with anti-Flag antibody. Immunoblot analyses of unpurified (lysate) and purified (eluate) protein extracts and SDS-PAGE of purified protein extract are presented. Note that SVBP (devoid of His-tag) was co-purified with all vasohibins but not with GFP. (**B**) Detyrosination activity of purified VASH2/SVBP complexes on purified brain microtubules or tubulin dimers assessed as in Fig. 2E. (**C**) Control by SDS-PAGE of non-assembled microtubule (tubulin dimers, Tub) or assembled microtubules (MT) used in Figs. 2E and S4B. MT and Tub extract (500 ng) were centrifuged 15 min at 25°C and 200,000 *g*. SN, supernatant. (**D**) Control by immunoblot of VASH1, VASH2 and SVBP amounts used in Figs. 2E and S4B.

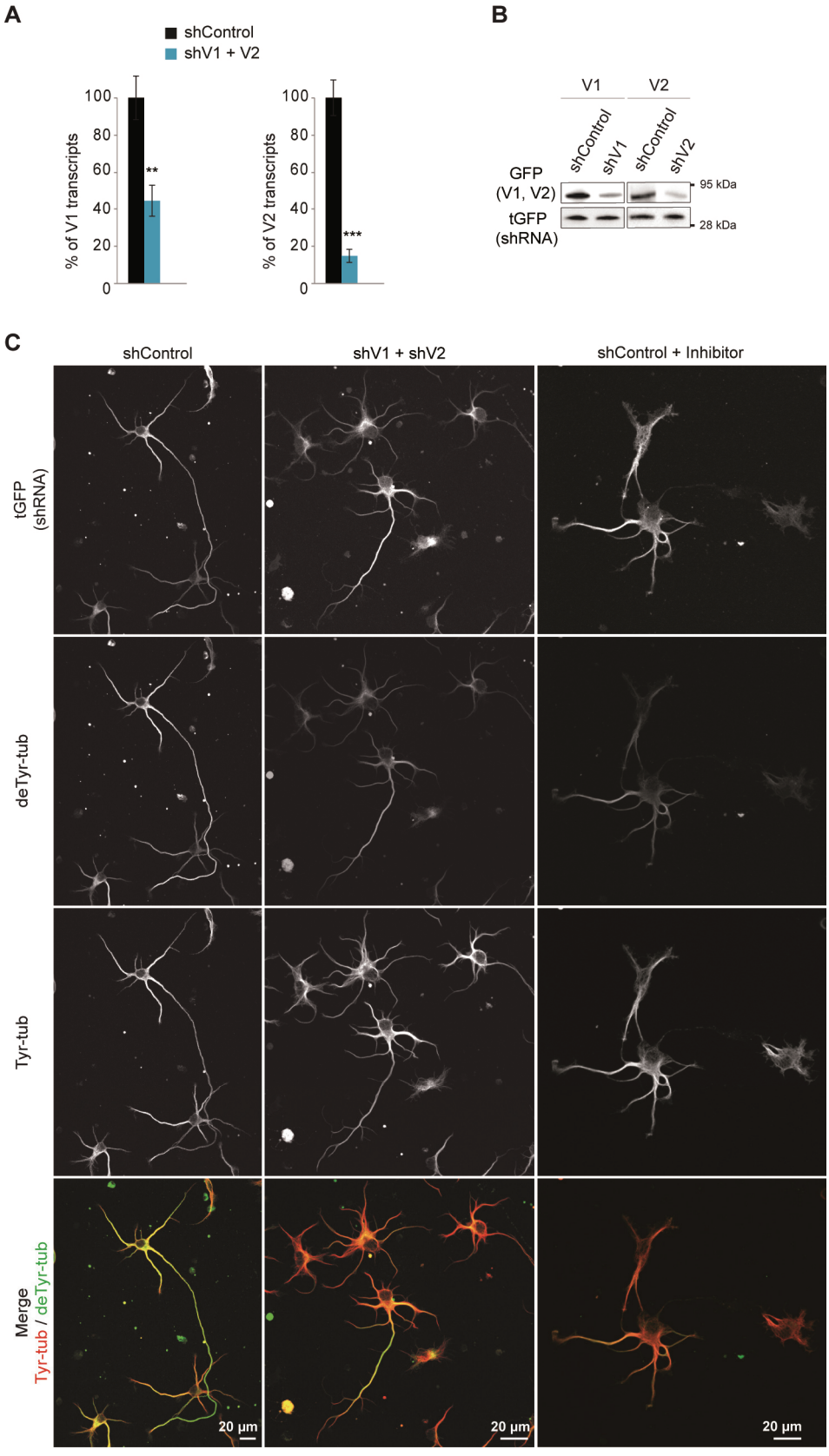

Fig. S5. Down-regulation of VASH1 and VASH2 affects neuronal differentiation. (**A, B**) validation of shRNAs targeting the vasohibins. (**A**) RT-qPCR quantifications of neuronal vasohibins transcripts in the presence of control or VASH1 and VASH2 shRNAs. Mean ± SEM.

Student t test: ** $p<0.01$ and *** $p<0.001$, n = 4. (**B**) HEK293T cells were co-transfected with plasmids allowing expression of each VASH and of the corresponding shRNA, or of a control shRNA. Crude protein extracts were analyzed by immunoblot with anti-GFP and anti-Flag to test the presence of VASH1/2 and with anti-turboGFP to assay the presence of shRNAs. (**C**) Merge and non-merged immunofluorescence images of Fig. 3D. Tyrosinated and detyrosinated α-tubulin levels were imaged at 2DIV using the same antibodies as in Fig. 2B. Levels of shRNA were imaged using an anti-tGFP antibody. Note that scale bars are different.

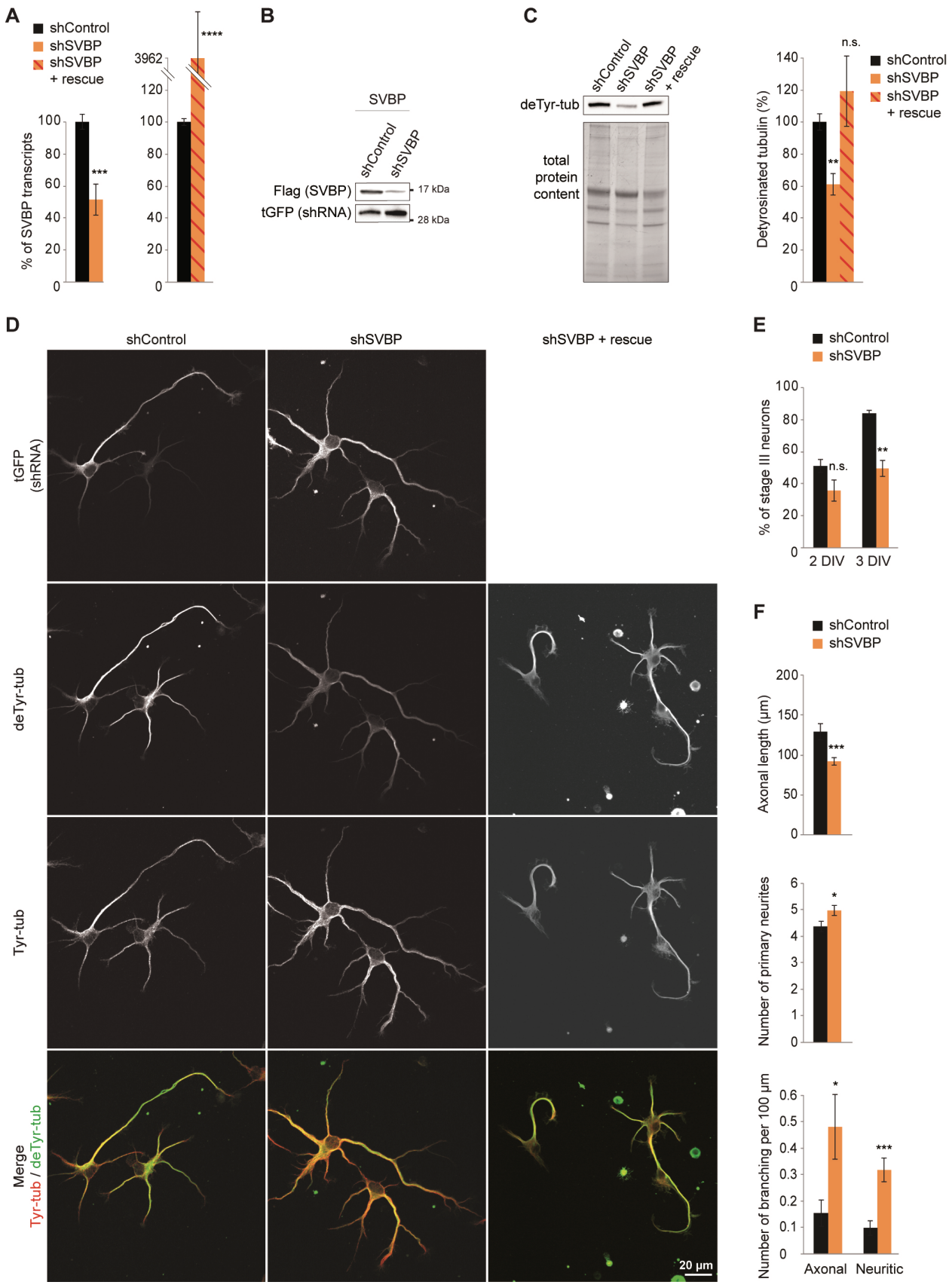

Fig. S6. Down-regulation of SVBP alters neuronal differentiation. (A, B) Validation of SVBP shRNAs. (**A**) RT-qPCR quantifications of neuronal *Svbp* transcripts in the presence of control or

SVBP shRNAs. Mean ± SEM. Student t test: *** $p<0.001$ and **** $p<0.0001$, n = 3-10. (**B**) HEK293T cells were co-transfected with plasmids allowing expression of the protein and of the corresponding shRNA, or of a control shRNA. Crude protein extracts were analyzed by immunoblot with anti-GFP and anti-Flag to test the presence of SVBP, and with anti-turboGFP to assay the presence of shRNAs. (**C**) Immuno-blot analysis of the effect of SVBP down-regulation with or without rescue on detyrosinated α-tubulin levels in neurons. Neurons were transfected by electroporation just before plating with plasmids allowing expression of shRNAs alone or shRNAs and a resistant form of SVBP, and analyzed at 2DIV. (right) Quantification of immunoblots. Results are expressed as percentage of detyrosinated tubulin related to shControl (duplicate immunoblots of independent neuronal cultures, mean ± SEM). Detyrosinated tubulin was significantly reduced in neurons transfected with shSVBP compared to neurons transfected with shControl, and rescued with shRNA-resistant SVBP (One way ANOVA with Sidak's multiple comparisons test, n = 6 for all, except for shSVBP ± rescue, n = 2). (**D**) Effect of SVBP down-regulation with or without rescue on neurite outgrowth and axonal differentiation of hippocampal neurons transfected as in C. Tyrosinated and detyrosinated α-tubulin levels were imaged at 2DIV using the same antibodies as in Fig. 2B. (**E**) Stage III neurons (bearing an axon) were counted manually on immunofluorescence images (generated as in B) from 3 to 4 different cultures at 2DIV and 3DIV (mean ± SEM, Student *t* test). (**F**) Morphometric analyses of at least 27 neurons (at 2DIV) using AutoNeuriteJ macro (see Material and Methods for details) on immunofluorescence images generated as in B (Student *t* or Mann and Whitney tests). n.s., not significant, * $p<0.05$, ** $p<0.01$, *** $p<0.001$, **** $p<0.0001$.

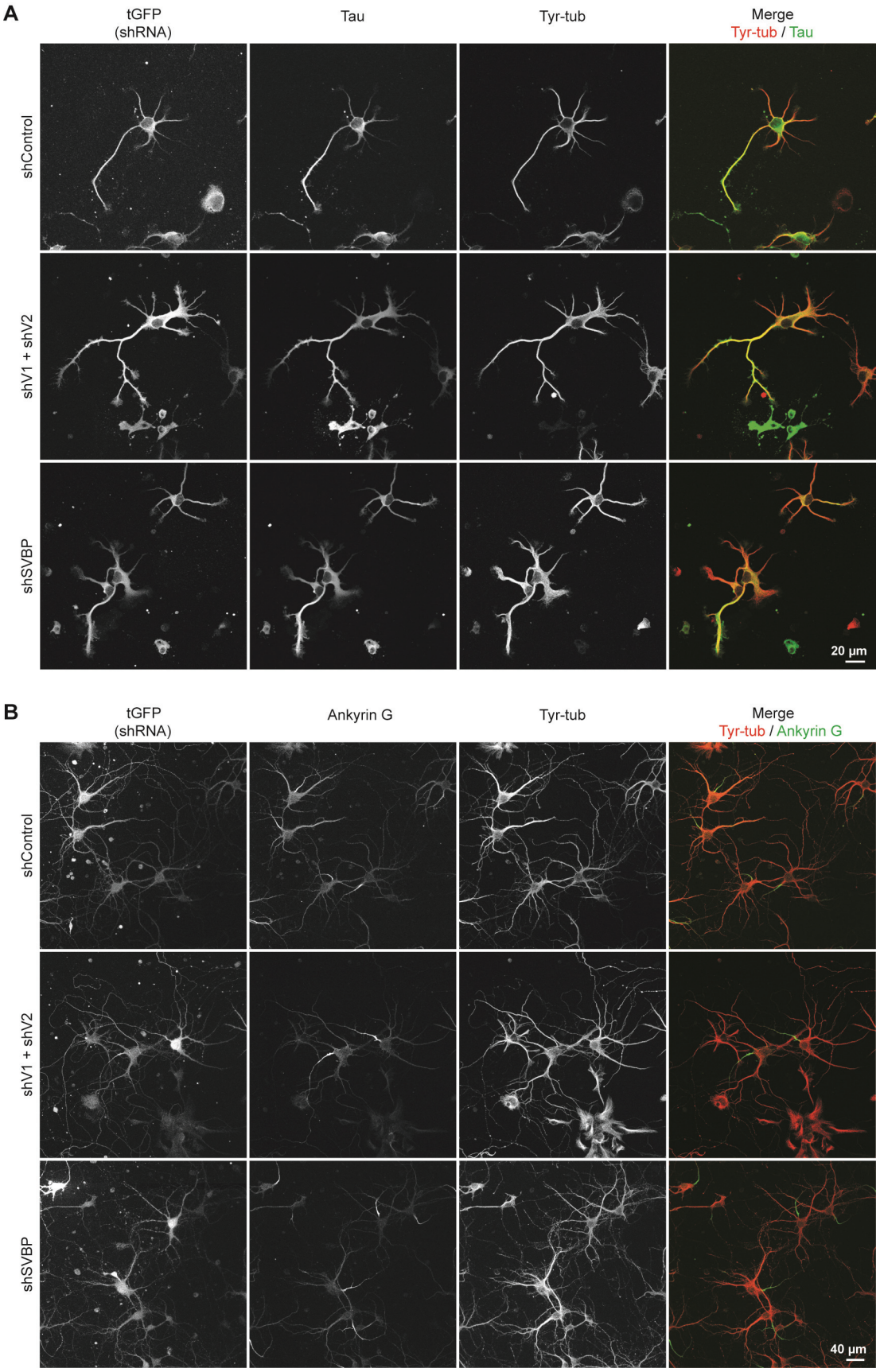

Fig. S7. Effect of vasohibins or SVBP down-regulation on Tau and ankyrin G staining of axons. Neurons were transfected by electroporation with shRNAs associated to turboGFP

(tGFP) cDNA just before plating and analyzed by immunofluorescence for tyrosinated tubulin and Tau contents at 3DIV (**A**) or for tyrosinated tubulin and ankyrin G levels at 10DIV (**B**). Levels of shRNA were imaged using an anti-tGFP antibody.

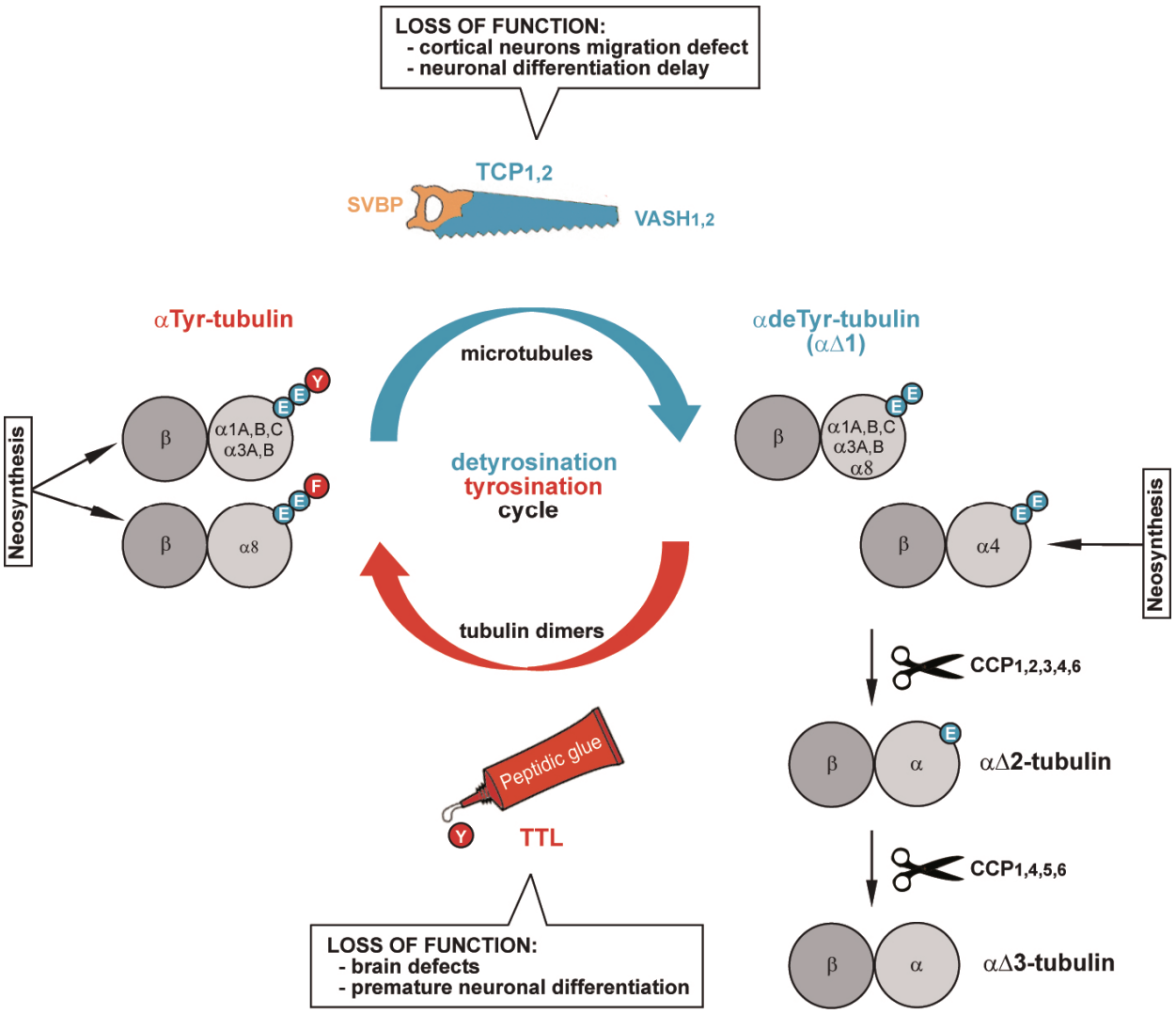

Fig. S8. Detyrosination/tyrosination cycle and implicated enzymes: a central position of tubulin carboxypeptidase (TCP). α-tubulin is usually neosynthesized with a C-terminal aromatic residue, tyrosine for most genes or phenylalanine for α8 gene (*34*). α-tubulin can enter into the de/tyrosination cycle when the αβ-tubulin dimer incorporates a microtubule and becomes a TCP substrate. TCP removes the last aromatic residue generating microtubule bearing detyrosinated α-tubulin (or αΔ1-tubulin). Detyrosinated α-tubulin pool can also be fed by the direct neosynthesis from α4 gene coding for an α-tubulin without last aromatic residue. To complete the cycle, the microtubule depolymerizes and liberates detyrosinated dimers which can be re-tyrosinated by tubuline tyrosine ligase (TTL). Whereas TTL enzyme consists of a single protein, TCP enzymes discovered in the present study comprise a catalytic unit (vasohibin) and an accessory protein (SVBP, small vasohibin-binding protein). Due to a duplication event of an ancestral vasohibin gene, vertebrates possess two TCP catalytic subunits, vasohibin-1 (VASH1) and vasohibin-2 (VASH2). Detyrosinated α-tubulin is the source of other modifications. Penultimate and ante-penultimate glutamate residues can be sequentially processed by the CCP family enzymes to generate αΔ2- and αΔ3-tubulin, respectively (*35-37*)

Peptide	Start	Stop	Best Mascot Score	TCP-R1	TCP-R2	TCP-R3
KVVPSGSSSASPNAAATTTAAAAAAAAAPHSGTK	6	39	27.48	1	-	-
VVPSGSSSASPNAAATTTAAAAAAAAAPHSGTK	7	39	58.66	2	-	1
RLETTEGASAQRDEEPEEEGEEDLR	40	64	44.40	2	-	-
DEEPEEEGEEDLR	52	64	92.22	2	-	1
DEEPEEEGEEDLRDGGVPFFINR	52	74	60.40	2	-	-
GGLPVDEATWER	75	86	59.10	3	-	1
IPIPSVPTFQPTTPVPER	114	131	69.72	3	2	1
IPIPSVPTFQPTTPVPERLEAVQR	114	137	42.11	3	-	-
ELQYNHTGTQFFEIK	141	155	53.71	1	-	-
SRPLTGLMDLAK	157	168	37.63	1	-	-
TYFSGNYFR	205	213	33.69	1	-	-
HIVLGVNFGGR	214	224	36.52	2	-	-
YGALGMSR	225	232	39.87	1	1	1
EDLMYKPPAFR	234	244	28.16	1	-	-
TLSELVLDYEAAYGR	245	259	83.16	3	-	1
LGQCVSHDPHSVEQIEWK	269	286	27.42	-	1	-
HSVLDVER	287	294	42.80	-	-	1
AMPDLSGYQIR	364	374	51.10	1	-	-
AMPDLSGYQIRV	364	375	48.64	1	-	-

Table S1. Vasohibin-1 peptides identified by mass spectrometry-based analysis (see Table S2 for detailed proteomic analyses). Numbering of start and stop amino acids is according accession number NP_796328. Numbers of spectral counts (SC) are indicated for each of the 3 independent fractions prepared using the clickable inhibitor (TCP-R1 to TCP-R3). Lower amounts of purified brain extract were used in R2 and R3 than in R1 (3- and 2-fold, respectively).

Table S2. Proteomic analyses of mouse brain clicked proteins (Auxiliary Table). The protein contents of 3 independently prepared replicates using either the clickable inhibitor (TCP-R1 to TCP-R3) or the unclickable inhibitor (Ctrl-R1 to Ctrl-R3) were analyzed by mass spectrometry-based proteomics. Lower amounts of purified brain extract were used in R2 and R3 than in R1 (3- and 2-fold, respectively). For each identified protein are given the entry, accession, protein and gene names extracted from the Uniprot knowledgebase, and the validated number of peptides (Pep), spectral counts (SC) and specific spectral counts (SSC) observed in each sample. Replicates with SSC = 0 despite SC > 0 were not considered (grey). To evidence proteins enriched in the replicates prepared with the clickable inhibitor, ratios of SSC (SSC TCP-R / SSC Ctrl-R) were calculated. Proteins exhibiting a SSC $\geqslant$ 3 and identified only in TCP samples or enriched at least 5 fold in TCP samples compared to corresponding Ctrl samples were considered as enriched in TCP samples (green). Among the 124 proteins enriched in TCP sample in at least one replicate, Vasohibin-1 (yellow) is the only protein enriched in all three replicates.